Climate to fish: Synthesizing field work, data and models in a 39-year retrospective analysis of seasonal processes on the eastern Bering Sea shelf and slope

Ivonne Ortiz[1,], Kerim Aydin[2], Albert J. Hermann[1], Georgina A. Gibson[3], André E. Punt[4], Francis K. Wiese[5], Lisa B. Eisner[2], Nissa Ferm[2], Troy W. Buckley[2], Elizabeth A. Moffitt[6], James N. Ianelli[2], James Murphy[7], Michael Dalton[2], Wei Cheng[1], Muyin Wang[1], Kate Hedstrom[8], Nicholas A. Bond[1], Enrique N. Curchitser[9], Charlotte Boyd[4]

[1] Joint Institute for the Study of the Atmosphere and Ocean, University of Washington, Seattle, WA 98195, USA
[2] Alaska Fisheries Science Center, NOAA, 7600 Sand Point Way N.E., Building 4, Seattle, WA 98115, USA
[3] International Arctic Research Center, University of Alaska Fairbanks, Fairbanks, AK 99775, USA
[4] School of Aquatic and Fishery Sciences, University of Washington, Seattle WA 98195-5020, USA
[5] Stantec Consulting Services Inc., 725 E Fireweed Lane, Anchorage AK 99503, USA
[6] Sea Star Scientific Editing, Seattle, WA 98115, USA
[7] Center for Studies in Demography and Ecology, University of Washington, Seattle WA 98195-3412, USA
[8] Institute of Marine Science, University of Alaska, Fairbanks, AK 99775, USA
[9] Department of Environmental Sciences, Rutgers University, New Brunswick, NJ 08901, USA

Corresponding author: Ivonne Ortiz
E: ivonne@u.washington.edu
P: 206.526.4692;
F: 206.526.6723

Keywords: Bering Sea, seasonal processes, end-to-end modelling, ecosystem modeling, pollock

Abstract

We combined field data and the output from a climate-to-fish coupled biophysical model to calculate weekly climatologies and 1971-2009 time series of physical and biological drivers for 16 distinct regions of the eastern Bering Sea shelf and slope. We focus on spatial trends and physical-biological interactions as a framework to compare model output to localized or season-specific observations. Data on pollock (≥8 cm) diet were used to evaluate energy flows and zooplankton dynamics predicted by the model. Model validation shows good agreement to sea-ice cover albeit with a one month delay in ice retreat. Likewise, the timing of spring phytoplankton blooms in the model were delayed approximately one month in the south and extend further into summer, but the relative timing between the spring and fall bloom peaks was consistent with observations. Ice-related primary producers may shift the timing of the spring bloom maximum biomass earlier in years when sea ice was still present after mid-March in the southern regions. Including the effects of explicit, dynamic fish predation on zooplankton in the model shifts the seasonal spring peak and distribution of zooplankton later in the year relative to simulations with implicit predation dependent only on zooplankton biomass and temperature; the former capturing the dynamic demand on zooplankton prey by fish. Pollock diets based on stomach samples collected in late fall and winter from 1982-2013 show overwintering euphausiids and small pollock as key prey items in the outer and southern Bering Sea shelf; a characteristic not currently present in the model.

The model captured two large-scale gradients, supported by field data, characterizing the overall dynamics: 1) inshore to off-shelf physical and biological differences with a gradient in inter-annual variability from higher frequency inshore to lower frequency offshore; and 2) latitudinal gradients in the timing of events. The combined effects of length of day, bathymetry, and tides, which are consistent from year to year, and the two large-scale gradients, characterize the environment on which regional differences were based and restrict their inter-annual and seasonal variability. Thus, the relative timing and sequence of events remained consistent within regions. The combination of model outputs and observational data revealed specific ecosystem processes: (1) The spatial progression in the timing, peaks and sequence of events over the shelf is driven by wind, sea ice, and stratification and creates a seasonal expansion and contraction of the warmer pelagic and bottom habitat suitable to pollock. (2) The seasonal warming of air temperature and the spring-summer expansion of the warm pelagic and bottom habitats influence

the ice retreat and the associated ice edge and open water spring blooms, as well as subsequent production/abundance of copepods and euphausiids. (3) These warmer conditions favor pelagic energy flows to pollock (≥10 cm) and allow their distribution to expand shoreward and northward along the shelf break. (4) The fall-winter expansion of the seasonal ice cover drives the contraction of warmer waters towards the outer and southwest shelf and favors benthic energy flows over most of the shelf. There, fall blooms allow for additional lipid storage by large copepods and euphausiids that sink close to the bottom where they either go into diapause or have a restricted diel migration over winter. (5) During these cold months, the preferred pollock habitat shifts and contracts towards the outer and southwest shelf where their increased density and reduced prey availability leads to winter pollock cannibalism and consumption of overwintering euphausiids. Our project highlights the benefits of linking continuous and long-term field work with the development and implementation of highly complex models. In the face of uncertainty, simulations such as these, tightly coupled to field programs, will be instrumental as testbeds for process exploration and management evaluation, increasing their relevance for future fisheries and ecosystem management and strategic planning.

1. Introduction

The volume and value of fisheries in the eastern Bering Sea (EBS) was over a billion pounds and 1.4 billion US dollars in product value in 2014 (Fissel et al., 2015). Large and numerous populations of seabirds and marine mammals are present and utilize this area for feeding and reproduction (Friday et al., 2012; Allen and Angliss, 2013; Denlinger, 2006). The EBS has experienced shifts in the physical environment in response to the 2000-2005 warm years (Stabeno et al., 2007), including changes to circulation (Stabeno et al., 2010; Danielson et al., 2012), the extent and duration of seasonal ice coverage and subsequent variability in bottom temperatures, stratification and mixed layer depth (Hunt et al., 2011; Stabeno et al., 2012a). These physical factors affect biological productivity (Hunt et al., 2011; Stabeno et al., 2012b), fish, seabird and marine mammal distributions (Friday et al., 2013; Hollowed et al., 2012; Hunt et al., 2014; Kotwicki et al., 2005; Mueter and Litzow, 2008; Ressler et al., 2014), predator-prey interactions (Livingston, 1989; Boldt et al., 2012, Hunt et al., 2014), and survival rates and reproductive success (Heintz et al., 2013, Hunt et al., 2016).

Climate variability, and in particular climate change under the global warming background (IPCC, 2007, 2013), impacts abundance, distribution, and the commercial catch of marine resources and has thus been recognized as one of the main challenges to sustainable fisheries (Brander, 2013; Salinger, 2013). Tools that resource management agencies have employed to understand the impact of climate change on the abundance, distribution and species composition of marine resources and fisheries include, but are not limited to, spatial models, single- and multi-species stock projections with environmental forcing and/or predator/prey interactions, and spatially-explicit ecosystem models (Hollowed et al., 2011, 2013). Diverse management measures have been implemented as part of an Ecosystem Approach to Fisheries Management (EAFM) for the Alaskan groundfish fisheries for over 15 years (Witherell et al., 2000). The general framework of the ecosystem assessment has evolved from that described by Livingston et al. (2005), to the current selected suite of physical-, biological- and fisheries-related ecosystem indicators that provide the core information for an annual ecosystem report card and ecosystem assessment chapter (e.g. Zador, 2015). A multi-model approach that includes multi-species models/reference points and ecosystem models, is used to simulate future ecosystem status and policy options (Jurado-Molina et al., 2005; Ianelli et al., 2016; Moffitt et al., 2016).

End-to-end models, which incorporate processes from climate to fish at various levels of complexity, have proliferated in recent years, and have become increasingly relevant as they improved to include human dimensions, climate impacts, and processes at multiple spatial and temporal scales (Travers et al., 2007; Rose et al., 2010; Punt et al., 2016). As a result, end-to-end models that include downscaled earth systems models coupled to lower trophic level models are starting to be more commonly applied to address fisheries-management concerns – especially those models that include key fish groups (Travers et al., 2009; Kishi et al., 2011; Rose et al., 2015; Travers et al., 2014a, b). End-to-end models have also been recognized as effective strategic tools and are considered essential to EAFM (Fulton, 2010; Fulton et al., 2014). Despite these advances, active research continues on refining our understanding of the linkages between climate variability and marine resources as mediated by oceanography and phytoplankton/zooplankton productivity.

As part of the Bering Sea Project, a large scale, multi-disciplinary, and multi-institutional ecosystem research program (Wiese et al., 2012), we developed (and coupled) ~10-km resolution models of the physics, lower trophic levels and key fish species in the Bering Sea. The Regional Ocean Model System (ROMS) applied to the Bering Sea (Bering10K) provides information such as currents, temperature, ice thickness and snow cover to the lower trophic level Nutrients-Phytoplankton-Zooplankton (NPZ) model developed under the Bering Ecosystem Study (BEST; ARCUS, 2004, 2005). The BESTNPZ model provides phytoplankton and ice-algae density estimates that were used to attenuate light in the Bering10K-ROMS model, thus establishing a two-way feedback between oceanography and lower trophic levels. In turn, the BESTNPZ model provides the zooplankton prey fields (euphausiids [Order Euphausiacea, krill], and small and large copepods [*Neocalanus* sp., *Calanus marshallae*, respectively]) to the Forage and Euphausiids Abundance in Space and Time (FEAST) fish model. Two-way feedback therein is enabled by applying the fish predation on zooplankton from the FEAST model to the zooplankton biomass in the BESTNPZ model. The spatially-explicit fisheries removals are included by sector, gear, and species (Fig. 1). The dual objectives for the coupled regional Bering10K-ROMS-BESTNPZ-FEAST models were to: 1) investigate biophysical processes and climate impacts; and 2) aid fisheries management by addressing both bottom-up and top-down forcing mechanisms on fish stocks and ecosystems (Wiese et al., 2012).

Here we describe the Bering10K-ROMS-BESTNPZ-FEAST model, and the physical and biological data used for comparison with, and validation of, the model output. We then present the weekly climatologies of physical and biological characteristics from a 1971-2009 hindcast of the model and highlight seasonal process in 16 distinct regions in the EBS shelf and slope. Finally, we present modeled monthly climatologies and length-based feeding habits of walleye pollock (*Gadus chalcogrammus* hereafter, pollock), based on stomach data collected from 1982 to 2013, and consider how pollock respond to the seasonal processes and shifts in energy flow within the food-web.

2. Methods and model descriptions

To facilitate the comparison and synthesis of spatial patterns in both data and model output, we use the set of standard marine regions developed by Ortiz et al. (2012) as part of the Bering Sea Project and encompass the EBS shelf and slope (Fig. 2). These marine regions were chosen based on documented similarity of selected meso-scale processes and the requirement to minimize within-region variance and maximize variance across regions. The inner, middle and outer domain are shown in light, medium and dark grey, respectively. In the southeastern Bering Sea shelf, the inner and middle domains are separated by the inner front (at approximately 50 m depth), while the middle and outer domain are separated by a middle transition zone (or middle front, approximately at 100 m depth) (Coachman, 1986).

The Bering10K-ROMS-BESTNPZ-FEAST model (Fig. 1) represents the three-dimensional dynamics of the two-way interactions between physical oceanography, nutrients-phytoplankton-zooplankton, fish and fisheries. The hindcast simulation covers the years 1971 to 2009. A detailed description of the regional downscaling to the Bering Sea is given by Hermann et al. (2013, 2016). Briefly, for the years 1971-2003, we used downscaled outputs from the coupled ocean-ice Coordinated Ocean Research Experiments (CORE; Large and Yeager, 2009) as atmospheric forcing, with oceanic boundary conditions interpolated from the ROMS model for the Northeast Pacific (NEP-5, Danielson et al., 2011). NEP-5 itself utilized CORE atmospheric forcing and ocean boundary conditions derived from the Simple Ocean Data Assimilation oceanic reanalysis (SODA, Carton and Geise, 2008). We used the Climate Forecast System Reanalysis (CFSR; Saha et al., 2010) for both atmospheric forcing and oceanic boundary conditions for the years 2004-2009 as described by Hermann et al. (2013). We describe the submodules of the Bering10K-ROMS-BESTNPZ-FEAST model in the following sections.

169 *2.1 Oceanography*

170 The Bering10K-ROMS is a regional coupled ocean-sea-ice circulation model whose spatial
171 domain is a subset of NEP-5, described and evaluated by Danielson et al. (2011). NEP-5 builds
172 on a model described by Curchitser et al. (2005). The Bering10K-ROMS uses a regular grid that
173 has a spatial resolution of ~10 km and 10 vertical layers. It extends from the western Gulf of
174 Alaska to the Russian coast and to slightly north of the Bering Strait (Fig. 2, see inset). The
175 Bering10K-ROMS simulation includes modifications to the heat and salinity fluxes of NEP-5,
176 which were calibrated using extensive mooring data (Hermann et al., 2013). Hermann et al.
177 (2016) describe additional modifications to the heat flux and ice dynamics, and conducted
178 additional model-data comparisons for temperature and salinity; it is that version of the physical
179 model which is utilized in the present work. Model coupling of the Bering10K-ROMS with the
180 BESTNPZ model includes feedback from the BESTNPZ to the Bering10K-ROMS model
181 through phytoplankton density, which affects attenuation of shortwave radiation, and thus heat
182 absorption in the upper water column (further described in Hermann et al., 2016).

183 *2.2. Nutrients, Phytoplankton and Lower Trophic levels*

184 The BESTNPZ model used is based on Gibson and Spitz (2011). It was specifically designed
185 to incorporate the impact of ice on lower trophic levels of the Bering Sea, and includes nutrients
186 (nitrate, ammonium, iron), ice algae, small and large phytoplankton, small copepods, oceanic and
187 shelf large copepods, oceanic and shelf euphausiids, jellyfish (Class Scyphozoa), fast and slow
188 sinking (pelagic) detritus, benthic detritus and benthic infauna (Fig. 3). Zooplankton are
189 distributed throughout the water column (only the large copepods vertically migrate), and
190 biomass is tracked for micro and mesozooplankton. In the BESTNPZ model, the lifespan of
191 euphausiids is implicitly a year (but has been recorded to be longer in higher latitudes,
192 [Dalpadado and Skjoldal, 1996; Hunt et al., 2016]) because their biomass (as for all the
193 zooplankton groups) approaches zero every winter. Both mortality and respiration exceed
194 growth, reflecting the understanding of euphausiid biology in the region when the model was
195 initially constructed rather than the more recently understood overwintering dynamics (Orlova et
196 al., 2014; Huenerlage et al., 2015). Spatio-temporal dynamics of the BESTNPZ model are
197 affected by ice thickness, temperature, salinity, solar radiation, and circulation patterns provided
198 by the Bering10K ROMS model (Fig. 1). The compartments used as food supply for fish in the
199 FEAST model are the euphausiids, copepods and benthic infauna (Fig. 3).

200 The total mortality of zooplankton groups and benthic infauna is modeled as a tuned
201 quadratic function of temperature and zooplankton biomass when the BESTNPZ model (Gibson
202 and Spitz, 2011) is not coupled to the FEAST model. When the Bering10K-ROMS, BESTNPZ
203 and FEAST models are fully coupled, zooplankton mortality is a combination of fish predation
204 calculated using the fish length-based bioenergetics model (section 2.3), and an additional 'other
205 natural mortality' that is a reduced value of the quadratic mortality utilized in the uncoupled
206 version. It is assumed that fish can prey on zooplankton throughout the water column so fish
207 consume zooplankton from all layers proportional to their layer-specific density even though the
208 FEAST model has no vertical fish distribution.
209
210 *2.3 Fish*
211 The FEAST model is a 2-dimensional (2D), gridded, daily-scale multispecies length-based
212 foraging, bioenergetics movement, and recruitment model for post-larval forage and predatory
213 fish. It runs within the Bering10K-ROMS framework, with fish as state variables being tracked
214 as 2D biological tracers. Fish numbers, condition factor and caloric density are driven by inputs
215 of prey availability, depth-averaged temperature, and water movement (i.e. advection) from the
216 Bering10K-ROMS-BESTNPZ model. The depth-averaged temperature is used in temperature-
217 dependent functions for prey-consumption and metabolism (Fig. 1). FEAST obtains daily
218 estimated dry weight of euphausiids, small copepods, large copepods, and benthic infauna from
219 the BESTNPZ model and produces daily mortality rates for prey, which can be fed back into the
220 BESTNPZ model as biomass consumed by fish for each zooplankton species and benthic
221 infauna. This results in a two-way coupled modeling structure between plankton and fish. The
222 conversion from BESTNPZ dry weight to FEAST wet weight and caloric density is calculated
223 according to pre-specified species-specific ratios. This is because there is no way of allocating
224 consumption to growth, reproduction and increased caloric density for biomass pools without
225 introducing *a priori* assumptions regarding the effects of environmental factors. Table 1 lists the
226 species included in the version of FEAST described here. FEAST also models spatially-
227 distributed fleet-specific fisheries, driven by historical spatial reconstructions of Bering Sea
228 fisheries on a weekly resolution.
229
230 *2.3.1 Fish population dynamics and foraging*

231 Each fish species in FEAST is divided into length bins. For some species, a separate set of
232 length bins are used for each fish-age class, covering ages 0 through 10+; for others, there is no
233 tracked age structure (Table 1, Fig. 4). For fish age-1 and older, 4 cm width fork length bins are
234 used; for age-0 fish or fish without age structure, 2 cm width fork length bins are used. All fish in
235 a length bin are assumed to have the midpoint length for that bin. All fish in the model,
236 including the smallest age-0 length bin (0-2 cm), are considered "post-larval" (discussed below).
237 Three state variables are tracked at each horizontal ROMS grid location for each fish-length
238 bin: 1) numbers of fish per m^2; 2) individual fish wet weight (tracked as condition factor, a ratio
239 representing deviation from an established fixed length/weight relationship); and 3) fish caloric
240 density (joules per gram of fish wet weight).
241 For each daily time step and each length bin of fish, the model first calculates the available
242 prey for that length bin of fish as the sum of the prey's biomass (across all prey, including
243 zooplankton and other fish bins) multiplied by a length- and species-based selectivity function
244 (gamma selectivity based on the log of the ratio between predator and prey lengths; Kinzey and
245 Punt 2007). For zooplankton, we used fixed mean prey lengths based on pollock stomach
246 samples collected in 2009-2010 (Buckley et al, in prep).
247 The daily consumption, respiration, and therefore net growth (in joules) for each fish length
248 box is calculated using a visual foraging model (e.g. Ware, 1978), which is based on the
249 available prey, combined with a temperature-dependent bioenergetics model of respiration
250 (Cianelli et al., 1998). This output is used to calculate the ideal "foraging activity level" for the
251 predator by assuming this activity level is linked to swimming velocity (affecting the amount of
252 energy captured) and respiration (affecting the cost of capture). The combination of prey length-
253 based selectivity and foraging energy maximization allows the model to capture "emergent"
254 prey-switching behavior.
255 Once daily rates (e.g. consumption, respiration) are calculated, net fish growth is computed
256 within the model either by transitioning a proportion of numbers of fish per unit area from a bin
257 to a larger length bin (representing growth in length), or by increasing condition factor (and
258 therefore weight-at-length) or caloric density (and therefore caloric density-at-length) according
259 to an allocation schedule adjusted to match historical data. Net energy losses are dealt with either
260 by decreasing condition factor or caloric density (fish cannot decrease in length). If the condition
261 factor or caloric density for a particular fish-length bin drops below a minimum, the fish starve

and are removed from the model (numbers of fish per m^2 set to zero). Mortality rates are then applied to the prey in the model given the amount of consumption calculated. While the rates are calculated daily, the state variables may be integrated on a finer timestep to match concurrent physics or BESTNPZ simulation. However, this does not imply that FEAST is designed to produce sub-daily results (e.g., diel feeding is not included).

Finally, the spawning biomass for an age-structured species in a grid cell is calculated by applying length-based maturity and fecundity curves to each length bin. "Spawning" fish convert caloric energy to "eggs" according to a fixed seasonal reproductive schedule from laboratory data (Buckley and Livingston, 1994). A fixed mortality rate is applied to the total number of eggs estimated from spawning fish. The surviving "eggs" for a species are modeled as a single quantity for each 2D cell and do not interact with other species or experience mortality, but are advected by water-column averaged velocities based on the underlying physical model. Within each cell, a proportion of the number of eggs is converted to numbers of fish age-0 across a fixed range of dates annually, at which point the fish are normally distributed across the smaller 2 cm size bins (out of 20).

2.3.2 Fish movement

Fish movement between neighboring horizontal grid cells is based on fish length, the spatial gradient of habitat quality and a diffusion rate inversely proportional to the local habitat quality (i.e., the steeper the habitat gradient, the faster fish swim towards the higher quality habitat). Due to the numerical integration timestep and the coarseness of the grid (10 km), there might be isolated instances when a small fraction of fish moves across grid cells faster than their swim speed. Habitat quality for each fish-length bin is defined as a function of net change in fish population energy, itself a product of individual net energy gain and predation mortality expressed in the same units. It is important to note that this "swimming rate" is not linked to the foraging effort (swimming velocity) mentioned above.

2.3.3 Fishing effort allocation

Fish can disappear from the model due to natural mortality or starvation, as explained above, but also due to fisheries. The fishing effort allocation for the hindcast is based on historical sector/gear/species catch data downscaled to weekly removals by Alaska Department of Fish and Game STAT6 statistical areas. Standard ADFG STAT6 areas are 0.5 degree latitude by 1.0

degree longitude when no land masses intersect (ADFG, 2009). The nominal STAT6 areas around land masses (e.g., the Alaska Peninsula) are irregularly shaped to conform to the land mass boundary and often much smaller than standard STAT6 areas. A uniform grid of standard size STAT6 covering the extent of the Bering grid was created to simplify the spatial distribution of catches. Land-free STAT6 areas were not affected by this, but irregular STAT6 areas were assigned to the overlapping STAT6 areas from the uniform grid (Boyd et al., 2014). Removals in each uniform STAT6 area were further downscaled to the FEAST grid (in this case the horizontal Bering10K grid), by allocating removals proportional to the biomass at the start of each week in each FEAST grid cell.

Catch input from historical data is in biomass by species. This is converted to removal rates (reduction rates in numbers) for particular fish length bins using fixed gear/species length selectivity curves generated from stock assessments. The fisheries are specified by sector (catcher-processors and catcher-vessels), target species and gear. The fisheries included are: catcher-processor for pollock trawl, Pacific cod trawl, pots and longline, other species trawl, pots and longline, herring gillnets and seine.

2.4 Initial conditions and field data

Although the fish can move throughout the total grid, the area of interest is restricted to the EBS shelf/slope regions, with a depth cutoff of 200 m for the shelf and 3,500 m for the slope. The northern shelf boundary corresponds to the U.S. Exclusive Economic Zone, and the farthest southwest (Aleutian) point corresponds to 172°W along the Aleutian Archipelago (Fig. 2). This area is seeded with fish for the initial conditions. The FEAST model needs starting conditions for each of three state variables: 1) numbers of fish per m^2; 2) individual fish wet weight; and 3) fish caloric density for each fish species. For all fish, the initial condition factors were assumed to be 1 and initial energy density was assumed to be the mean caloric density-at-length. Initial conditions for the fish were derived from the historical database of the RACE (Resource Assessment and Conservation Engineering Division) Bottom Trawl summer Survey (BTS) conducted by the Alaska Fisheries Science Center (AFSC) and stock assessment estimates in the case of pollock, cod, arrowtooth, and herring. When needed, stock assessment estimates were scaled in proportion to the biomass in the BTS that fell outside the assumed distribution of the fish stock in the stock assessment used (e.g., arrowtooth estimates were scaled down to account for fish in the Aleutian Islands). The numbers of fish-at-age were converted to numbers of fish-

323 at-age and -length based on long term length distributions for each age estimated from a
324 historical database maintained by the AFSC Resource Ecology and Fisheries Management
325 division's Age and Growth Program (http://www.afsc.noaa.gov/REFM/Age/). For the initial
326 conditions, we allocated the number of fish-at-length estimated for 1971 from the stock
327 assessment using the mean spatial distribution by length derived from the BTS based on
328 "average" years (1996, 2000, and 2006). The warm/cold/average year classification follows
329 Stabeno et al. (2012), who defined "average" years as those when daily and monthly water
330 column temperatures were close to their corresponding 1995-2010 mean at mooring M2. If no
331 fish of a given size were recorded at the station in the BTS corresponding to a location in the
332 model, then the number of initial fish for that bin at that location was set to zero. No adjustment
333 was made for length selectivity of the BTS. Total biomass for species with no age structure was
334 allocated using the mean spatial biomass distribution in the BTS of average years scaled by a
335 catchability factor estimated from survey biomass estimates and the group's biomass as
336 estimated by an ecosystem mass balance model for the EBS (Aydin et al., 2007). Total numbers
337 of fish per m^2 for species with no stock assessment were estimated based on survey data: total
338 BTS biomass as scaled by the catchability, converted to numbers of fish-at-length. For this
339 conversion we assumed a length-based population structure at equilibrium and multiplied it by
340 the corresponding longterm length-weight relationships. Table 2 summarizes the source
341 information for the initial conditions.
342
343 *2.5 Model simulation*
344 The Bering10K-ROMS-BESTNPZ models were initialized using time-specific conditions from
345 the hindcast by Hermann et al. (2016), which uses the same model parameterizations. We started
346 the model on July 1, 1970, and ran a simulation with fish movement, but no mortality or growth,
347 through December 31, 1970 (fish spin-up). Starting January 1, 1971 the fish mortality and
348 growth were turned on for the remainder of the simulation (Jan 1, 1971 - December 30, 2009). A
349 forcing file containing daily catches by sector, gear, species, and length for each grid cell
350 supplied the catch data for the calculation of the fishing effort. A second forcing file supplied the
351 estimated age-1 recruits from the (EBS area-integrated) stock assessment for pollock, Pacific cod
352 and arrowtooth flounder. At the start of each year, the total number of age-0 fish (estimated
353 based on fecundity of mature fish and distributed according to the location of spawning fish),

were corrected to that of the stock assessment estimate, while preserving the spatial distribution of the model output. Due to a lack of sufficient data on life history rates and movement, the population structure of species with no stock assessment was assumed to be static; species with no length structure were considered sessile.

2.6 Data and model validation

First we evaluated the model performance for physics, phytoplankton, and pollock. We focused model-data comparisons on key physical and biological parameters, namely sea-ice cover, chlorophyll-*a* concentrations, and timing of spring and fall blooms at moorings 2, 4, 5, and 8 (M2, M4, M5 and M8, see Fig. 2 for locations). The moorings have been described in detail in Stabeno et al. (2012a, b) and are maintained by NOAA/Pacific Marine Environmental Laboratory, with the first mooring (M2) deployed in 1995. We also compared the annual number of age-1 and older pollock from the FEAST outputs to those estimated by the stock assessment for the EBS pollock (Ianelli et al., 2011). Second, since our model includes fish, we addressed whether adding fish predation makes a difference in the zooplankton biomass as estimated using only quadratic mortality.

2.6.1 Sea-ice

We used data presented in Sigler et al. (2014) to compare with weekly sea-ice cover model output to examine sea-ice variation along the 70-m isobath. This dataset is based on data from the National Ice Center (NIC), which covers the period 1971-2005 and from the Advanced Microwave Scanning Radio-EOS for the period 2002-2012. The values from both data series are very similar for the overlap years 2002-2005 (Stabeno et al., 2012b), and the average of both datasets was used. A box of 100 km x 100 km was defined around each of the four moorings, and daily values were computed from 1996-2009 and weekly averages derived. Ice was present all years at moorings M8 and M5, but was absent at M4 during 2001 and 2005, and at M2 during 1996, 2001, and 2003 - 2005 (Sigler et al., 2014).

2.6.2 Chlorophyll-a concentrations

We used daily averages of shallow (~10 m) chlorophyll-*a* concentration (Chl*a*, mgC/m^3) for the period 1996-2009 from Sigler et al. (2014) to estimate weekly averages. The data are fully

385 detailed in Sigler et al. (2014). Briefly, the time series focuses on mooring data at 11 m (or the
386 shallowest instrument at M5 and M8) and additional chlorophyll-*a* fluorescence measurements
387 and water samples taken during hydrographic casts conducted when the moorings were deployed
388 and recovered. Both moored and hydrographic chlorophyll-*a* fluorescence (volts) were converted
389 to chlorophyll-*a* concentration ($\mu g\ l^{-1}$) using factory calibration (which has significant error).
390 Chlorophyll-*a* estimates based on fluorescence sensors were compared to those from the water
391 samples taken during the hydrographic casts for quality control of the mooring-based
392 measurements; unusual values or irregular spikes were excluded as were data where
393 measurement drift occurred.
394
395 *2.6.3 Timing of Spring and Fall Bloom*
396 We compared the time-series of the weekly total phytoplankton biomass (ice algae, large and
397 small phytoplankton, gC/m^2) of the top 10 m as estimated by the model to the corresponding
398 time series of chlorophyll-*a* estimates presented by Sigler et al. (2014) to evaluate model
399 performance in the timing of the spring and fall bloom, as well as their relative magnitude. Time
400 series were based on values at the mooring locations (M2, M4 between 1996-2009, M5 and M8
401 between 2004 and 2009). We use the temporal thresholds for determining spring and fall blooms
402 proposed by Cheng et al. (2016) to identify the time of spring and fall bloom maxima: spring
403 blooms are those occurring on or before Julian day 200 (or week 29); fall blooms are those
404 occurring on or after Julian day 230 (week 33). These thresholds are 20 days later than those
405 used by Sigler et al. (2014) based on the observational data to account for the delay in ice retreat
406 in the model (Julian day 180 for spring bloom and 210 for fall). The 30-day interval between is
407 the same (Cheng et al., 2016).
408
409 *2.6.4 Pollock Abundance*
410 We evaluate FEAST model performance for the abundance of age-1 and older pollock by
411 comparing the total modeled number of fish age-1 and older by year from 1971-2009 to the
412 number of fish as estimated for the same period by the pollock stock assessment for the EBS
413 (Ianelli et al., 2011). The time-series of modeled numbers-at-age were calculated by extracting
414 the model output corresponding to regions 1 through 16 (Fig. 2), the assumed distributional area
415 for the EBS pollock. We focus on pollock abundance as a key validation because they comprise

the largest fish biomass in the EBS, and are the primary consumers of zooplankton (Aydin et al., 2007).

2.6.5 Difference between one-way and two-way feedback for NPZ-FEAST coupling

To determine the impact dynamic fish predation can have on modeled zooplankton biomass, we computed and then compared weekly climatologies of aggregated zooplankton (large copepods and euphausiids) within the primary habitat for pollock (>20 cm), for both one- and two-way feedback simulations (see section 2.2). Primary habitat is defined as the area between 2°C and 6°C (Barbeaux, 2012) in regions 1 through 9.

2.7 Analysis – Weekly climatologies of physical and biological model output

Weekly climatologies of physical and biological variables for the 16 standard marine regions (Fig. 2) were calculated for the 1971-2009 fully coupled (including fish predation) modeled time series. Averages by Julian week were used, resulting in a final week of each year being 8 days (9 in a leap year). The physical variables evaluated included: fraction of sea-ice cover and depth-integrated temperature. The biological variables included biomass of: ice algae, large and small phytoplankton, microzooplankton, small copepods, large oceanic/shelf copepods, and euphausiids. All variables constitute integrated values per m^2 over the upper 300 m (or the total depth of the water column, whichever was shallower). Weekly anomalies for the 1971-2009 time-series for the 16 regions were also calculated for the euphausiid biomass in the upper 300 m as well as for the depth-averaged temperature in the upper 300 m.

2.7.1. Monthly and seasonal climatologies of copepods, euphausiids and pollock in stomach samples of pollock length 8-80 cm

There are no direct zooplankton observations in the Bering Sea in winter and so the model assumes that biomass approaches zero and are thus not available for consumption by fish. To evaluate the concordance between model assumptions and observed availability of large zooplankton to pollock, we used information from pollock stomach samples collected throughout the year on the eastern Bering Sea shelf and slope by a variety of surveys from 1982 to 2013. This also serves the purpose of establishing a baseline year-round availability of zooplankton. The fish food habits database is maintained by the Resource Ecology and Ecosystem Modeling group of the NOAA/AFSC (http://www.afsc.noaa.gov/REFM/REEM/Data/default.htm). The data were allocated to the corresponding marine region in Fig. 2 based on the haul location

where the samples were collected. First, we computed the monthly averages of frequency of occurrence of pollock, copepods (any size), and euphausiids in pollock diets for each region with at least 100 samples in any given month. Then, we calculated the seasonal contribution of each of these three prey categories to pollock diet as a function of predator (pollock) length in each region where there were at least 300 samples for each seasonal diet. Seasons were defined as the corresponding quarter in a year: Jan-Mar (winter), Apr-Jun (spring), Jul-Sep (summer), and Oct-Dec (fall).

3. Results and discussion

We present and discuss results in three sections: the first section addresses model performance; the second addresses the data from the pollock stomach samples; and the third section addresses the weekly climatologies for modeled physical attributes, phytoplankton and zooplankton, across regions.

3.1 Model performance

3.1.1. Sea-ice cover

Danielson et al. (2011) showed NEP-5 closely reproduces ice cover (expressed as percent ice concentration) and spring ice retreat onset. Model outputs for depth-integrated temperature at two southern moorings (M2 and M4) run slightly warmer in winter (up to 2°C, Figure 4 of Hermann et al., 2016), though near-surface temperatures can be colder than observed in the northern Bering Sea (Hermann et al., 2016). Weekly climatologies of area averaged sea-ice concentration from satellite data and the Bering10K-ROMS-NPZ-FEAST model simulations are shown in Figure 5 for the 100 km x 100 km boxes around each mooring site. Measured and modeled ice cover are maximal between weeks 6 through 19 (Feb-May), with maximum ice cover increasing from south to north (M2 to M8). When sea ice is present, averaged sea-ice cover typically remains below 50% in the south (M2, M4) and is usually above 50% in the north (M8) and in the transition area (M5). Although the onset of sea ice retreat in the model matches observations, the model is generally not ice free until mid-June to early July at all moorings. Whereas observations, on average, show sea-ice cover is gone between week 17 (late April) at M2 and week 24 (mid-June) at M8. The difference between observed and modeled sea-ice cover at M8 ranges between 38% and 1%. The model also calculates the onset of ice cover one (M2, M4, M5) or two (M8) weeks earlier than observed.

476 The late ice melt delays the timing of the spring bloom (Fig. 6). Cheng et al. (2016) evaluated
477 spring and fall blooms in the eastern Bering Sea using output from the ROMS-NEMURO-NEP
478 model, and suggested the lack of ice algae in the NEMURO model (Kishi et al., 2007) as one
479 potential contributing mechanisms to the slower sea-ice retreat. Our BESTNPZ model has an ice
480 module that explicitly includes ice algae as well as feedback between the phytoplankton density
481 and shortwave absorption. This suggests the slow sea-ice retreat is probably caused by other
482 internal model features as suggested by Danielson et al. (2011), (e.g. the ice code utilized by
483 Bering10K and NEP-5 had sea ice melting only at the ice-ocean interface but not at the ice-
484 atmosphere interface), or may be inherited from global climate models used for atmospheric
485 forcing and boundary conditions, as suggested by Cheng et al. (2016).
486
487 *3.1.2. Spring and fall bloom relative magnitude and timing*
488 Annual time series of weekly mean observed chlorophyll-*a* (Chl*a*, mgC/m^3) and total
489 modeled phytoplankton (large + small) biomass (gC/m^2) at four moorings are shown in Fig. 6
490 (top two rows). In general, the model shows interannual variability of phytoplankton biomass
491 evident in the observations, albeit the magnitudes and timing differ from observations. The
492 relative onset and peak of the modeled spring bloom compared to observed data is generally on
493 time for the north moorings M5 and M8, where spring blooms are ice-related; we note the
494 blooms tend to last longer in the model compared to the observed data. In contrast, the peak
495 biomass of spring blooms at M2 and M4 can be either ice-related (earlier in the year) or open
496 water (later in the year when ice retreated early) (Sigler et al., 2014). These two types of blooms
497 show up in the climatology at M2 and M4 based on chlorophyll data (bottom row Fig. 6), but is
498 clearly not captured in the model, as shown by the weekly climatology of total phytoplankton
499 biomass. In the model, the timing of ice algae does indeed happen earlier in the year compared to
500 the timing of either small or large phytoplankton, however its biomass is so small it gets
501 overwhelmed and thus has little effect on the timing of the spring bloom. The climatology of the
502 fall bloom based on data, shows a north to south gradient in both its timing and magnitude. It is
503 almost nonexistent at M8 (north) but it progressively increases and occurs later at M2 where the
504 fall bloom can reach spring-like magnitudes. In contrast, the modeled fall bloom always has a
505 magnitude matching or exceeding that of the modeled spring bloom. These discrepancies in the
506 timing of the blooms seem partly due to the difference between the observed and modeled timing

of ice retreat, where modeled sea-ice retreat is delayed in the spring, and the onset of sea ice is earlier in the fall. The interval between the timing of the maximum spring bloom and the maximum fall bloom is similar between the observed data and the modeled climatologies, however the modeled blooms appear to have a longer duration.

In general, the spring-to-fall ratio of maximum phytoplankton biomass in the model is either lower or inverse compared to the spring-to-fall ratio of the observed chlorophyll-*a* (rows 3 and 4 in Fig. 6). Both time series potentially have biases. For the model time series, lower spring maxima than those in fall could result from low values of ice algae biomass in early spring, high biomass values of small phytoplankton in fall (Fig. 6, bottom 2 rows), or a combination of both. In the observed data, the mean maximum spring chlorophyll-*a* concentration is always higher than the fall maximum, and the spring to fall ratio increases towards the north as fall blooms in the north tend to have a lower magnitude than in the south. The latitudinal gradient in the observed data might be overestimated due to: the lack of data during 1996-2003 at M5 and M8, and/or the likely biased Chl*a* measurements based on factory calibrations using spectral fluorescence signals defined on different phytoplankton communities or different physiological states of the phytoplankton (Escoffier et al., 2014) than those in the EBS at time of sampling. In general, neither the observed magnitude of the spring-to-fall peak biomass ratio, nor its latitudinal gradient, is adequately captured by the model.

The phytoplankton biomass in the model could further be biased due to: high assumed doubling rates; the emergent low grazing rates by micro-zooplankton; overestimation in nutrient availability; and/or an oversimplification of fixed carbon to chlorophyll-*a* for each phytoplankton size group, which does not permit an evolution in the ratio of carbon to chlorophyll-*a* within a species group as environmental conditions change. The influence by light, cell size, and other factors on the quantitative relationships between the C and Chl*a* needs to be incorporated into the model. Lomas et al. (2012) estimated an average C:Chl*a* ratio of 50, in spring and summer of 2008 and 2009, regardless of sampling depth, cell size or nutrient status; when the samples were parsed by depth, size or nutrient status, the average values did vary according to expectations (e.g. small cells, <5μm, had a higher C:Chla ratio than large cells, >5μm), but the differences were not significant. Even if assumed significant, the difference in the C:Chl*a* ratios of large and small cells are insufficient to specify the difference in magnitude between the maximum spring (mostly large cells) and fall blooms (mostly small cells). Moreover, using higher fixed C:Chl*a*

538 ratios for small phytoplankton and lower C:Chl*a* ratios for larger phytoplankton would still not
539 address the latitudinal gradient in the maximum spring to fall bloom observed in the data.
540 Regardless of the mechanism leading to the low ice algae and high small phytoplankton
541 biomass in the model, the ratio among the primary producers is biased and their total biomass, as
542 calculated in the model, is likely lower in early spring and higher in fall than it should be. Both
543 the difference in the timing of the blooms, as well as the overestimated ratio of the spring versus
544 fall phytoplankton biomass, are evident regardless of whether comparisons are based on Chl*a*,
545 satellite images http://www.science.oregonstate.edu/ocean.productivity/standard.product.php or
546 net primary production derived from ocean color estimates (Brown et. al., 2011).

547 *3.1.3. Spring bloom timing and sea ice retreat*
548 The model did not replicate the late ice-retreat early-spring bloom maxima behavior, despite
549 capturing the seasonal variability of the timing of ice retreat. We explore this discrepancy further
550 in Figure 7 using scatterplots of the timing of maximum spring bloom (defined as the Julian
551 week when Chl*a* or phytoplankton biomass was at its maximum during spring) versus timing of
552 sea-ice retreat (defined as the week when sea-ice cover fell below 15%). The top row in Figure 7
553 shows the scatter plots using the observed data from Sigler et al. (2014). Chlorophyll-*a*
554 measurements do not provide any information on the autotrophs contributing to the chlorophyll
555 pool, so rows 2 to 5 (Fig. 7) show the timing of the maximum phytoplankton biomass in spring
556 of ice algae only (row 2), large phytoplankton only (row 3), the sum of ice algae and large
557 phytoplankton (row 4), and the sum of small and large phytoplankton (row 5). The timing of the
558 maximum spring phytoplankton biomass was related to the timing of ice retreat at M8 and M5,
559 regardless of which primary producers were included in the calculation (note only years with
560 Chl*a* measurements from Sigler et al., (2014), were plotted, but when all modeled years 1996-
561 2009 were considered, the pattern holds). Only the timing of maximum ice algae biomass
562 responded to the timing of the ice retreat in the model at all moorings, including M2 and M4;
563 none of the other combinations of primary producer biomass showed a response in their timing
564 to that of the ice retreat. In one out of three cases the timing of the peak small+large
565 phytoplankton biomass was later than that of large phytoplankton alone. This suggests that ice
566 algae biomass (or ice-related primary producers) can influence the onset of spring bloom if sea
567 ice is present. The data used in Sigler et al., (2014, appendix) show that in the south, where sea
568 ice may or may not be present, the timing of the spring bloom can be either driven by ice-related

blooms overlapping with open-water blooms or there can be an interval between an ice-related bloom and open water bloom, or in the absence of sea ice, there are only open water blooms and their timing is delayed until late spring. This validates the inclusion of ice-related primary producers included in the model, albeit their role needs to be tuned so that their biomass or dynamics within the model can indeed shift the timing of the spring bloom to an earlier date when late there is late ice retreat. Another mechanism preventing a shift to an earlier spring bloom in the model are the small phytoplankton, which might be increasing too fast in late spring and their high biomass is shifting the maximum biomass of total phytoplankton later in the year. More studies on the community composition of primary and secondary producers during late winter and early spring are needed to elucidate the extent to which ice-related plankton communities differ from or interact with late spring communities, their role in nutrient depletion and the food availability for copepods and euphausiids as they come out of diapause and overwintering.

3.1.4. Number of pollock

The number of pollock, age-1 and older, at the start of the calendar year is calculated by the FEAST model and from the stock assessment (Fig. 8). Age-1 fish in the FEAST model are corrected at the start of the year to match those from the stock assessment (Ianelli et al., 2011), while the numbers of fish from the older ages are a result of survival as calculated in the model. In general, the FEAST model calculates a slightly lower number of total fish as compared to the stock assessment (Ianelli et al., 2011). The difference appears to be due to a higher mortality on incoming age-1 (now age-2) pollock in FEAST model as well as higher fishing mortality on fish >50 cm. The first is partly due to the limited number of zooplankton over winter in the model, to which pollock respond with an increase in cannibalism and starvation. While this has been observed (see results for pollock stomach samples in section 3.1.6), the effect is exacerbated in the FEAST model. In addition, studies by Heintz et al. (2013) have shown that low lipid storage at the start of winter is an important factor that determines the survival of age-1 pollock. Whether this was a primary factor driving the lower recruitment observed in the model (as compared to stock assessment estimates) was not quantified. The bioenergetics and population structure are set-up such that these and other relationships such as zooplankton impacts on recruitment to age-3 (Eisner et al.,, 2014) would be emergent properties in the model. The higher fishing mortality is due to a lower weight-at-length in the model compared to that observed in the fisheries, which

leads to an overestimate of the absolute number of fish removed when converted from catch in tons.

3.1.5 Effect of fish predation on modeled seasonal zooplankton biomass (difference between one-way and two-way feedback between NPZ-FEAST)

Pollock is the main consumer of euphausiid and large copepod biomass. Figure 9 shows the weekly biomass in shelf areas within a 2 to 6°C temperature range for small and large copepods and euphausiids for 1971-2009, as predicted by the Bering10K-ROMS-BESTNPZ-FEAST model with one- and two-way coupling (as described in section 2.2). With one-way coupling, the temperature-dependent quadratic mortality in the BESTNPZ model is a closure term that assumes total mortality is proportional to biomass year round. In contrast, the model configuration with two-way coupling has zooplankton mortality due to fish predation (as simulated using the FEAST model), and "other natural mortality" as simulated by a reduced quadratic term. Including the modeled fish predation on the zooplankton dynamics captures the varying demand of zooplankton as prey by fish as a function of: predator length structure; location; increased metabolism; and relative availability of other prey. While the exact dominant mechanism is harder to isolate, in aggregate, the above factors provide the model with a varied suite of mechanisms to capture interannual and seasonal variability. The biomass of small copepods (Fig. 9, top panel), as calculated using dynamic fish predation, is lower throughout spring and early summer compared to the biomass calculated using quadratic mortality only. This is because small copepods are consumed quickly by small fish, particularly by small pollock, and it is not until fish have increased in length that other prey become available. A similar pattern is true for large copepods (Fig. 9, middle panel). The lower large copepod biomass calculated with two-way compared to one-way feedback reflects the higher consumption of copepods by fish during the spring and summer when they are most available. The demand for large copepods extends until late summer, as fish increasing in length feed less on small copepods and more on large ones. The higher consumption of copepods using two-way feedback releases the predation mortality on euphausiids, which then maintain a higher biomass throughout fall (Fig. 9 bottom panel) before overwintering. In the NPZ model, the zooplankton biomass is set to decrease until it is almost nil, so there are no overwintering euphausiids nor movement off-shelf of the large copepods. There is, however, a fixed date for start and end of diapause. When the zooplankton biomass of the various groups is shown for all areas across a

631 thermal envelope (2-6°C), it indicates that there can be a top-down control on zooplankton via
632 predation by fish. The fish predation on the different zooplankton groups varies annually and
633 depends on the time of year. The model keeps track of biomass in grams of carbon only,
634 meaning it cannot capture changes in energetic content, and does not allow for multiple
635 generations of euphausiids (documented for *T. longipes* in other areas [Iguchi and Ikeda, 2004]
636 and for *T. inermis* in the Barents Sea [Dalpadado and Skjoldal, 1996]). In addition, the model
637 does not take length of euphausiids into account so a change in biomass can be interpreted as
638 either a change in individual weight or a change in the number of individuals. Any of these
639 factors, however, would probably only slightly modify the difference in weekly biomass
640 computed using the different coupling modes.

641 *3.2 Climatologies by region*

642 Here we focus first on the weekly climatologies based on model output for physical
643 characteristics, primary producers, secondary producers and the 1971-2009 time series of
644 euphausiid biomass and temperature. We then present the monthly and seasonal climatologies of
645 pollock prey based on stomach samples.

646

647 *3.2.1 Physical characteristics*

648 Figure 10 shows the off-shelf to inner shelf and latitudinal gradient across selected regions
649 for duration of daylight, fraction of sea-ice cover and integrated water temperature in the upper
650 300 m or throughout the water column, whichever is shallower. The duration of daylight is
651 shown as a guide: spring equinox, week 12; summer solstice, week 26; fall equinox, week 38;
652 and winter solstice, week 51. Duration of daylight only varies by latitude, so the graphs are
653 repeated from off-shelf to the inner shelf. The fraction of ice cover increases from off-shelf to
654 inner shelf. A strong seasonal signal exists where the average duration of ice-free waters can be
655 as short as thirteen weeks in the north inner shelf (region 11) to near year round in the south, off-
656 shelf (region 16). Figure 10 (middle panels) shows the progression of ice cover, from north to
657 south and inner to off-shelf. Sea-ice retreat is slower in the model than in the observations, so the
658 duration of the ice-free season is underestimated over the middle shelf regions (see section
659 3.1.1). However, except for the timing, the north to south pattern and relative magnitude of ice
660 cover in the middle domain is very similar to that described by Stabeno et al. (2012a, see their
661 Figure 2) for moorings M2, M4, M5 and M8 along the middle shelf for the period 1972-2010.

The amount of sea ice in each shelf domain is controlled by different mechanisms: primarily advection forced by winds in the south middle shelf and melting; local production in the inner shelf in areas such as Bristol Bay (region 2) and near Norton Sound (region 11), and primarily formed and melting in the north (e.g. region 10) (Stabeno et al., 2007). The integrated ocean temperature shows relatively small seasonal variation in the mostly ice-free off-shelf region, where water remains stratified even during winter (Stabeno, et al., 1998; Overland et al., 1999). Increasingly higher seasonal variability is seen towards the inner shelf (Fig. 10, bottom row). The inner shelf is shallow (<50 m), and there is thorough mixing of the water column (Overland et al., 1999, Sullivan et al., 2014). The largest latitudinal difference appears to be along the middle shelf, where depth-integrated temperature typically falls below 0°C in the north, yet remains above 1°C in the south. Lauth and Kotwicki (2013) found a bottom temperature of 1°C to be a thermal limit for most groundfish of commercial importance on the Bering shelf. The seasonal changes in integrated temperature shown here suggest the inner shelf might be too cold for several groundfishes to overwinter in that area, and fish, including some sizes of pollock (see Figure 2 in Buckley et al., 2016), would probably move towards the outer shelf as winter sets in. The seasonal extent of the sea ice and colder temperature concentrates pollock towards the outer shelf in winter and influences the extent of their spawning grounds, which Petrik et al. (2015) found to influence the distribution of early life stages of pollock in the EBS and potentially their spatial overlap with predators.

3.2.2 Primary producers and microzooplankton

Weekly climatologies for modeled ice algae, large phytoplankton, small phytoplankton, and microzooplankton are shown in Figure 11 for selected regions across off-shelf to inner shelf and latitudinal gradients. The biomass values represent the vertically integrated values in the upper 300 m or entire water column, whichever is shallowest. The slower ice retreat and earlier onset of sea ice in the model compared to observations compresses the ice free period and delays the ice algae and spring bloom. However, the results are relevant in that they show the relative timing over cross-shelf and latitudinal gradients. Depending on year-specific conditions, ice algae can start the primary productivity cycle, which in turn influences the start of secondary production. Except for the delayed onset, the climatology of ice algae from the model output follow the general dynamics of ice-related blooms as described by Brown and Arrigo (2013).

693 The model shows higher ice algae biomass in the northern and outer ice-edge areas (Fig. 11), in
694 part because these areas have a higher and more prolonged ice cover (Fig. 10). In the middle
695 shelf, ice algae typically start at the southern ice edge as ice retreats, in early spring (region 3),
696 and peak in late spring north of St. Matthew Island (region 10).
697 We focus on the relative timing of large phytoplankton as opposed to the absolute magnitude
698 of the maximum biomass during spring blooms. The delay of the timing of the spring bloom
699 maximum biomass in the model (discussed in sections 3.1.2 and 3.1.3) is also evident in the
700 weekly climatologies across regions. The relative magnitude of the spring phytoplankton
701 biomass across the southern shelf follows the pattern described by Rho et al. (2007) and that of
702 Lomas et al. (2012) estimated using a vertically generalized, productivity model – the highest
703 primary production occurs in the middle shelf, decreasing towards the slope, with similar or
704 lower values observed in the inner and outer shelves. In the northern shelf, the modeled spring
705 phytoplankton biomass is lower for the inner than the outer shelf. The spring bloom starts off in
706 the southern middle shelf and progresses to off-shelf and inner shelf regions in agreement with
707 satellite images for March, April and May (Hunt et al., 2010), with the timing of the spring
708 bloom in the inner northern shelf regions occurring six weeks later on average. In the model,
709 high large phytoplankton biomass typically lasts for approximately three months. Small
710 phytoplankton begin to bloom several weeks after large phytoplankton. Small and large
711 phytoplankton peak closer in time in the northern and inner regions than in southern regions,
712 with less pronounced summer lows and slower decrease of phytoplankton biomass towards the
713 end of fall (see observed Chl*a* at M8, Fig. 6). This decreasing pattern is not captured for the
714 northern regions in the model; only the closer timing of the spring and fall bloom is captured. As
715 mentioned earlier, the model overestimates the biomass of small phytoplankton which drives the
716 fall bloom, and in turn may extend the growth period of zooplankton. This overestimation of the
717 fall bloom is systematic across the slope and shelf areas as compared to domain-based estimates
718 shown by Hunt et al. (2010), and when considering their contribution to total Chl*a* biomass. In
719 late summer (August and September), small phytoplankton usually make up 10 to 50% of total
720 Chl*a* biomass across the entire shelf and around 20% in the outer shelf (Eisner et al., 2016,
721 Figure 6 in their paper). Both large and small phytoplankton appear to fuel microzooplankton
722 (bottom panel, Fig. 11). Since the large and small phytoplankton blooms are typically separated
723 by a drop in biomass in early summer, regionally coherent patterns emerge despite the lagged

timing in the model and the interannual variability in the magnitude of the peak biomasses and the different physical processes driving the dynamics in the northern versus southern, and inner versus outer shelves (Stabeno et al., 2012a). The different spatial scales of the environmental variability of factors, such as the timing of ice retreat, vertical stratification and mixing across regions, means local conditions are not uniformly favorable or unfavorable across the shelf and slope, and biological responses may vary between regions while still having spatial coherence, as shown by Eisner et al. (2016, see their Table 2). This applies to both differences between the north and the south, which have uncorrelated warm/cold years (Stabeno et al., 2012b; Luchin and Panteleev, 2014) and within the north and the south, as cross-shelf differences such as bathymetry and tidal currents buffer or intensify the impact of environmental factors.

3.2.3 Secondary producers

The spatial coherence and timing sequence is evident in the 1971-2009 mean weekly biomass for the small copepods and euphausiids (Fig. 12). The peak biomass of small copepods is shortly followed by an increase in the biomass of large copepods and euphausiids. As with phytoplankton, these increases occur later in the model than the observations, but in both progresses towards the northernmost and inner shelf regions. Model estimates here have several biases. In addition to the overall delay in the reproductive/growth cycle, large copepods are probably underestimated in magnitude and seasonal availability. The seasonal availability is shortened on both ends: the delayed reproduction/growing cycle due to the delayed timing of the spring blooms and the early diapause imposed by a fixed start date; each attenuate dynamic responses to favorable environmental conditions. Copepod biomass has been observed to peak in fall (Eisner et al., 2014), but this is not possible in the model set-up used here. A revised version of the NPZ model is currently being evaluated using alternative set-ups. A better understanding of the mechanisms driving the onset or termination of copepods diapause and quantitative relationships between environmental factors and diapause timing would also improve future models. The large oceanic copepod biomass in the offshore area increases after diapause. This increase in biomass is likely a model artifact and not something that occurs in reality, as: i) it is coming entirely from deep-water layers, where small concentrations of copepods are magnified by the integrated sum due to the expanding thickness of the deep layers; and ii) no other zooplankton groups show corresponding trends (see Fig. 12, first column). The earlier timing of

755 the increase in euphausiid biomass in the model output for the outer shelf and off-shelf areas
756 resembles that of the dominant species in the outer shelf, *Thysanoessa inermis*, which spawns in
757 April. Likewise, the later biomass increase in the middle shelf would be akin to spawning of
758 *T. raschii*, which occurs mid- to late-May (Vidal and Smith, 1986; Smith, 1991) and may extend
759 to at least August, when collected individuals had spermatophores, indicating they were breeding
760 (Hunt et al., 1996). The fall increase in the biomass of small copepods and euphausiids in the
761 model output seems to be driven, at least partially, by the fall phytoplankton bloom. However,
762 we did not quantify the relative contribution of microzooplankton versus phytoplankton to the
763 biomass increase of either small copepods or euphausiids.
764 The increase in both phytoplankton and zooplankton biomass in the fall is evidence that
765 sufficiently favorable conditions may occur to support large fall blooms, albeit their frequency is
766 overestimated in this model. Mid- to late-fall increases in plankton biomass can be highly
767 important for the ecosystem as they would allow for a longer period of lipid storage for young
768 pollock (Heinz et al., 2013), can favor a longer growing season for copepods (Morata and
769 Søreide, 2015) and lipid storage for both copepods (Tsuda et al., 2001) and euphausiids (Harvey
770 et al., 2012). However, few data exist for this time of year because most surveys end by early fall
771 (Eisner et al., 2014, 2016). The importance of euphausiids as prey for pollock over the late fall
772 and winter cannot be overstated, and a longer growing and lipid storage season would translate
773 into higher quality prey.
774
775 *3.2.4 Variability in euphausiid biomass by region*
776 Because of the importance of euphausiids as year-round prey for pollock, we show the entire
777 1971-2009 time series of weekly anomalies of integrated temperature and euphausiid biomass for
778 selected regions in Figure 13. The model assumes river runoff is the same temperature as the
779 receiving oceanic waters. However, rivers may discharge warm water, as is the case of the
780 Yukon River (Dean et al., 1989). In Figure 13, the inner shelf is shown at the top transitioning to
781 off-shelf at the bottom. Within each shelf domain, we show time series for a region in the north
782 and one in the south, top to bottom. Results from a hindcast simulated with a previous version of
783 the Bering10K-ROMS-BESTNPZ model (Hermann et al., 2013) found that large crustaceans
784 (*Neocalanus* and euphausiids) tended to covary inversely to temperature on the outer shelf. A
785 more rigorous analysis of the observed temperature and euphausiid biomass as estimated by

786 acoustic surveys was conducted by Ressler et al. (2014), but others have also made similar
787 observations from field data (Hunt et al., 2011; Coyle et al., 2011). Inverse covariance between
788 large crustacean abundance and temperature appears to be stronger during the recent string of
789 warm (2001-2005) and cold years (2007-2013) than during the earlier years, but is particularly
790 evident in off-shelf/slope areas (regions 15 and 16 in Fig. 13). Years prior to 1977 had a weaker
791 inverse covariance, and Hermann et al. (2013) reported a positive correlation between
792 temperature and large crustacean zooplankton on the inner and northern shelf. This tendency in
793 the north and inner areas may be linked to changes in the dominant water mass and to flow
794 reversals due to wind-driven currents (Danielson et al., 2012). In the inner domain, the
795 temperature anomalies show higher variability, disrupting what would be a multi-year monotonic
796 trend in other areas and highlighting the differences in timing and magnitude of warm/cold years
797 in the north compared to the south shelf. While this might be influenced by the dominant water
798 masses, the main factor is likely the timing of ice retreat and river runoff. We did not conduct
799 any analysis to evaluate whether it is current variability that interrupts the monotonic trend
800 observed elsewhere. Another off-shelf to inner shelf gradient in the physics (which affects the
801 zooplankton), is the higher frequency interannual variability towards the inner shelf, with lower
802 frequency variability towards the off-shelf areas. A spectral analysis conducted by Hermann et
803 al. (2016, Figures 18 and 19 in their paper) confirms 1-2 year interannual variability in the inner
804 shelf (top portion Fig. 13), while interannual variability is characterized by processes of typically
805 2-4 years frequency in the off-shelf (lower portion Fig.13). This partly explains why the off-shelf
806 area is much more stable year-round than the inner shelf. Other processes influencing the
807 frequency of the variability include: ice expansion and retreat over the shelf, but lacking in the
808 basin; strong advection in the outer shelf that removes the ice signal; and winds in shallow areas
809 which can mix the entire water column, while in the off-shelf, winds mix only the upper water
810 column (above 20 m) and the water column remains stratified throughout the year (Stabeno et
811 al., 1998).

812 *3.2.5 Euphausiids, copepods and pollock as prey of pollock*

813 Pollock diet data for fish 8 mm – 80 mm collected over 30 years are summarized for selected
814 regions (n = 58,403) in Figure 14. The monthly frequency of occurrence of euphausiids,
815 copepods and pollock in pollock stomachs show copepods have a strong seasonal availability
816 (primarily spring and summer), while euphausiids remain an important prey throughout most of

817 the year, with a possible peak in late fall as well as in the spring (Fig. 14, 1st column; see also
818 Buckley et al. [2016] for complete prey composition by length and area). This is likely due to
819 their continued availability: while copepods go into diapause and remain near the bottom (Baier
820 and Napp, 2013), euphausiids overwinter; they have a restricted vertical migration and may also
821 switch to detrital and benthic feeding (Sargent and Falk-Petersen, 1981; Huenerlage et al., 2015),
822 making them accessible to pollock as part of the hyperbenthos. In any given year, the available
823 euphausiid biomass is the result not only of the reproduction and growth of the year's cohort, but
824 is likely multi-generational (Dalpadado and Skjoldal, 1996). Interannual patterns also indicate
825 that during the summers when copepods are less available, pollock do not increase their
826 consumption of euphausiids (Buckley et al., 2016). The importance of copepods to summer
827 feeding success, and pollock size-related patterns in summer feeding migration relative to
828 geographic distributions of copepods and euphausiids (Buckley et al., 2016) explains why
829 pollock biomass is not a reliable predictor of euphausiid abundance and why pollock predation
830 on euphausiids does not necessarily result in top down control, as noted by Ressler et al. (2014).
831 However, Hunt et al. (2016) noted a strong negative relationship between euphausiid biomass
832 and pollock biomass. More studies are needed to evaluate the relative abundance of copepods
833 with respect to euphausiids and how top-down control of euphausiids by pollock may be
834 attenuated by relative availability of copepods as prey and other factors. The decreased
835 availability of copepods is at least partly substituted by the increased cannibalism during late fall
836 and early winter. The occurrence and the amount of cannibalism is highest where the distribution
837 of large and small pollock overlap (Boldt et al., 2012, see Fig. 7 of Buckley et al., 2016 for
838 example of distribution of pollock by length). Cannibalism by pollock is particularly high in the
839 south middle shelf (region 3) in winter, in the outer shelf during spring and summer (region 8),
840 and is most widespread in fall. Given the importance of fall conditions for determining pollock
841 survival in the model, direct measurements of mid- to late-fall zooplankton could be very
842 influential. The contribution of euphausiids, copepods and small pollock to the pollock diet is
843 supplemented by local zooplankton communities and other larger prey. While euphausiids were
844 not evaluated by Eisner et al. (2014) since sample collection was conducted during daylight
845 when euphausiids were located too close to the sea floor to sample quantitatively, their results
846 show *Calanus* spp. were in higher abundances in middle and outer shelf regions than in the inner
847 shelf during August to September. These taxa are responsible for most of the large copepod

biomass, which matches the presence of large copepods in diets of pollock greater than 20 cm. Likewise, mysids and shrimp in the southeastern Bering Sea were in highest concentrations in the inner shelf, which seems to match with diet data (although shrimp are also present in diets elsewhere on the shelf) (Buckley et al., 2016).

4. Summary and conclusion

Understanding the processes that lead to spatiotemporal variability in the flow of energy from primary production through successive trophic levels is key to predicting potential effects of climate change on upper trophic levels and commercially important species. While overall trends in primary and secondary production are indeed relevant as indicators of maximum energy available for transfer in the system, it may be that pockets of high prey abundances or more suitable temperatures provide a spatial energetic refuge for forage and upper trophic levels. Our results are in agreement with Buckley et al. (2016), showing that pollock might feed on copepods more and on euphausiids less than previously believed (Ressler et al., 2012). If so, the succession of zooplankton blooms and length of availability of copepod versus euphausiid prey (growing season versus year-round, respectively) might be equally influential in driving pollock survival and/or distribution, than considering only their abundance. The seasonal and interannual availability of necessary resources – or the lack thereof – contributes to the success or failure of particular age classes or reproductive seasons.

As flows of available prey and energy vary seasonally, it is important to understand how and when these resources become available to upper trophic levels, and the role of their location within the water column. For example, vertical, horizontal and temporal distribution are important mechanisms for niche partitioning, allowing for spatial overlaps or mismatches, not only for fish and zooplankton, but also seabirds and whales (Russel et al., 1999; Harvey et al., 2009; Hunt et al., 2014; Siddon et al., 2013; Sigler et al., 2016). Because of the implications that climate variability may have on primary and secondary production, it is important to understand driving factors prone to change – such as temperature, sea-ice cover timing and duration, winds and currents – and distinguish them from those that will keep their current pattern such as length of day, bathymetry, and tidal currents. For example, vertical mixing in shallow (<30 m) areas is primarily influenced by tidal mixing whereas in the middle and outer shelf where tidal currents are weaker, wind-driven mixing and thermal stratification play a major role. Hence vertical

879 mixing in the middle and outer shelf is potentially more susceptible to climate change than in
880 shallow areas. Similarly, tidal currents are three times stronger in the southern than in the
881 northern Bering Sea shelf (Stabeno et al., 2012a), meaning the northern shallow areas may be
882 more susceptible to future changes in vertical mixing than those in the south. Assuming
883 northward winds and temperature will increase in the future, the position of the middle front
884 would be more susceptible to change than that of the inner front. Based on the forecasts by
885 Hermann et al. (2016), preliminary analyses show that the spring bloom, which is driven by
886 physical changes, may shift to an earlier time in the north, and to a later time in the south.
887 The spatiotemporal patterns of the physical and biological characteristics addressed in this
888 paper are emergent properties of the model. We use its general coherence with observed patterns
889 as a basis to synthesize processes in the EBS shelf and slope environment, during warm and cold
890 months (after Stabeno et al., 2016) as shown in Figure 15. Sea-ice cover (itself driven largely by
891 wind in the northern Bering Sea; Stabeno et al., 2007) serves as a primary driver of both bottom
892 and pelagic habitat by creating a higher water density cold pool that serves as a thermal boundary
893 (Lauth and Kotwicki, 2013). Both ice cover and the cold pool expand and contract seasonally
894 (Wyllie-Echeverria and Wooster, 1998), concentrating pollock (20-59 cm long) towards the
895 outer shelf and slope (Buckley et al., 2016; Kotwicki et al., 2005) at their maximum extent
896 during cold months (November to March, winter and early spring). Ice cover contracts over
897 spring months and the cold pool progressively contract northward throughout the warm months
898 (May to September, late spring and summer). In spring as the ice melts, the ocean warms and
899 water stratifies (Niebauer et al., 1995; Sullivan et al., 2014), and primary and secondary
900 production (Stabeno et al., 2010) and pollock follow. Prevailing features during warm months
901 include: a) sea-ice absence and retreat; b) stronger fronts and weaker across-shelf water
902 exchange (Stabeno et al., 2016), higher local nutrient regeneration/recycling of nitrate (Cheng et
903 al., 2016), (although episodic uncoupling of the nitrogen cycle can lead to nitrite accumulation,
904 Mordy et al., 2010; c) weak variable winds (northeastward on average) over the shelf (Danielson
905 et al., 2012); and d) warm saltier water advected northward by the Anadyr Current in the north
906 (Coachman et al., 1975; Wang et al., 2009). During October, a transition month (early to mid-
907 fall), depth-averaged temperature begins to decrease, and the mixed layer begins to deepen on
908 the southeastern shelf (Sigler et al., 2014). Large-scale physical processes shift to their typical
909 cold months (winter-early spring) features: a) advance of ice; b) weak frontal structure on the

910 shelf (Coachman, 1986; Stabeno and Hunt, 2002) that allow cross-shelf wind driven flow,
911 favoring nitrate replenishment in the southern shelf (Stabeno et al., 2016); c) increasingly
912 southwestward winds over the shelf, strengthening through December (Danielson et al., 2012);
913 d) in the north, cold salty water is advected eastward by winds (Coachman et al., 1975; Wang et
914 al., 2009). While there is spatial coherence among contiguous regions, conditions do not vary
915 shelf-wide in the same proportion due to the spatial variability of these large scale physical
916 processes (Eisner et al., 2016; Luchin and Panteleev, 2014; Stabeno et al., 2016). Zooplankton
917 and pollock are finely tuned to this system. Seasonal energetic sources for euphausiids switch
918 from pelagic phytoplankton and zooplankton in the spring and summer to the benthos in fall and
919 winter while copepods go into diapause (Baier and Napp, 2013). Seasonal energetic sources for
920 pollock switch from pelagic zooplankton in the spring and summer to stored energy from lipids,
921 overwintering euphausiids, and cannibalism in the fall and winter. The spatial progression in the
922 timing, peaks and sequence of events throughout the shelf, as well as regional and length specific
923 pollock diets, are coherent with a seasonal expansion and contraction of pollock distribution, and
924 support the feeding and spawning migration routes for pollock (Buckley et al., 2016; Kotwicki et
925 al., 2005, 2015).
926 Some of the most beneficial aspects of the model hindcast described here have been the
927 syntheses it has prompted, how it has provided a year-round framework for local or seasonal
928 observations, and how it has helped identify gaps, guiding research both in the design and
929 temporal focus of surveys. Recent improvements to the models presented here already have a
930 tighter link to benthic energy sources and sinks and improved ice dynamics. Other
931 simplifications, such as no diel migration by euphausiids and no overwintering in the
932 zooplankton dynamics, are being addressed. These modifications, as well as increasing the
933 growing season for copepods, will impact the calculated values for movement, diets, survival and
934 growth of pollock (and other fish) in the model. The small phytoplankton and microzooplankton
935 biomass will likely be re-evaluated as well. As our understanding of the variability and plasticity
936 of life history strategies within each of these multi-species groups increases, the modeling
937 framework will evolve to incorporate the more important differentiating characteristics.
938 Multidecadal projections such as those conducted by Hermann et al. (2016) have shown potential
939 changes in habitat (cold pool) as perceived by groundfish. The ability to run simulations of

integrated ecosystem models has proven a necessary tool to elucidate potential costs and benefits of management strategies, as well as future challenges (Fulton, 2011; Fulton et al., 2014).

Our project highlights the benefits of linking continuous and long-term field work with the development and implementation of highly complex models. Models such as these serve as tools to identify information gaps, test process hypotheses, and prioritize research. They are essential to a coordinated understanding of the linkages and responses between co-varying environmental factors, climate variability, and fish dynamics – an increasingly pressing need within resource management. In the face of uncertainty, simulations such as these tightly, coupled to field programs, will become more common as testbeds for process exploration and management evaluation, increasing their relevance for future fisheries and ecosystem management and strategic planning.

Acknowledgements

The authors would like to acknowledge the collective contribution of all the researchers involved in the Bering Sea Project who generously shared data and expertise. Ed Farley, Patrick Ressler, Mike Sigler, Cal Mordy, George Hunt, two anonymous reviewers, and the guest editor, Phyllis Stabeno, are thanked for their comments and insights on earlier versions of this paper. IO, AJH, AEP, EM and JM were partially supported by the North Pacific Research Board (NPRB) as part of the Bering Sea Integrated Ecosystem Research Program (BSIERP projects B52, B70, B71 and B73). MW, NB, WC, EC and KH, were partially supported by National Science Foundation grant number 0732534; GG was funded by NSF awards ARC-1107203 and ARC-0732538. FKW was fully supported by NPRB in his former role as Science Director and Modeling Manager for NPRB. This work was partially funded by JISAO under NOAA cooperative agreement NA100AR4320148; NSF grant: "Bering Sea Ecosystem Study" (NSF-0732534). This research is contribution No. 4286 from NOAA/ Pacific Marine Environmental Laboratory, contribution EcoFOCI-0873 to NOAA's Ecosystems Fisheries-Oceanography Coordinated Investigations, publication 597 from the North Pacific Research Board; and 169 from the BEST-BSIERP Bering Sea Project. This publication is partially funded by the Joint Institute for the Study of the Atmosphere and Ocean, University of Washington, contribution No. 2016-01-19.

970 **References**

971 ADFG, 2011. ADF&G Groundfish/Shellfish Statistical Areas, Chart 3 – Bering Sea. 2nd Ed.,
972 March 2011. http://www.adfg.alaska.gov/static/fishing/PDFs/commercial/chart03_bs.pdf
973 Allen, B.M., Angliss, R.P., 2012 Alaska Marine Mammal Stock Assessment, 2012. U.S. Dept.
974 Commer. NOAA Technical Memorandum NMFS-AFSC-245. 282 p. downloaded 05/2013
975 http://www.nmfs.noaa.gov/pr/sars/pdf/ak2012.pdf.
976 ARCUS, 2004. Bering Ecosystem Study (BEST) Science Plan. Arctic Research Consortium of
977 the U.S, Fairbanks, AK 82 pages.
978 ARCUS, 2005. Bering Ecosystem Study Program (BEST) Implementation Plan. Arctic Research
979 Consortium of the U.S, Fairbanks, AK 43 pages.
980 Aydin, K., Gaichas, S., Ortiz, I., Kinzey, D., Friday, N., 2007. Comparison of the Bering Sea,
981 Gulf of Alaska, and Aleutian Islands Large Marine Ecosystems through food web
982 modeling. NOAA Technical Memorandum NMFS-AFSC-178.
983 http://www.afsc.noaa.gov/Publications/AFSC-TM/NOAA-TM-AFSC-178.pdf
984 Baier, C.T., Napp, J.M., 2003. Climate-induced variability in *Calanus marshallae* populations. J.
985 Plankton Res. 25, 771-782.
986 Barbeaux, S.J. 2012. Scientific acoustic data from commercial fishing vessels, eastern Bering
987 Sea walleye pollock (*Theragra chalcogramma*). Thesis (Ph.D.) University of Washington.
988 219 pp.
989 Boldt, J.L., Buckley, T.W., Rooper, C.N., Aydin, K., 2012. Factors influencing cannibalism and
990 abundance of walleye pollock (*Theragra chalcogramma*) on the eastern Bering Sea shelf,
991 1982-2006. Fish. Bull. 110, 293-306.
992 Boyd, C., Dalton, M., Ianelli, J., Murphy, J., Punt, A.E., 2014. BSIERP: Integrate models of
993 pollock and cod. North Pacific Research Board Final Report B71, 58 p.
994 Brander, K., 2013. Climate and current anthropogenic impacts on fisheries. Climatic Change.
995 119, 9-21.
996 Brown, Z.W., Arrigo, K.R., 2013. Sea-ice impacts on spring bloom dynamics and net primary
997 production in the eastern Bering Sea. J. Geophys. Res. 11, 1–20.
998 http://dx.doi.org/10.1029/2012JC008034.

Brown, Z.W., van Dijken,G.L., Arrigo, K.R., 2011. A reassessment of primary production and environmental change in the Bering Sea. J. Geophys. Res. 116, C08014. http://dx.doi.org/10.1029/2010JC006766.

Buckley, T.W., Grieg, A., Boldt, J.L., 2009. Describing summer pelagic habitat over the continental shelf in the eastern Bering Sea, 1982-2006. NOAA Technical Memorandum NMFS-AFSC-196. 49p. http://www.afsc.noaa.gov/Publications/AFSC-TM/NOAA-TM-AFSC-196.pdf.

Buckley, T.W., Kappler, K., Ressler, P.H., Aydin, K.A., Hibpshman, R.E., Jones, D., McCarthy, A., *In prep*. Comparisons of pollock diets from midwater and bottom trawl surveys, and comparisons of net-caught and pollock-consumed euphausiids in 2009 and 2010 in the EBS

Buckley, T.W., Livingston, P.A. 1994. A bioenergetics model of walleye pollock (*Theragra chalcogramma*) in the Eastern Bring Sea: Structure and documentation. NOAA Technical Memorandum NMFS-AFSC-37. http://www.afsc.noaa.gov/Publications/AFSC-TM/NOAA-TM-AFSC-37.pdf.

Buckley, T.W., Ortiz, I., Kotwicki, S., Aydin, K., 2016. Diet composition of walleye pollock in the eastern Bering Sea, 1987-2011, and predator-prey relationships with copepods and euphausiids. Deep-Sea Res. II. 00, 00–00, this issue.

Carton, J.A., Giese, B.S., 2008. A reanalysis of ocean climate using Simple Ocean Data Assimilation (SODA), Mon. Wea. Rev. 136, 2999-3017.

Cheng, W., Curchitser, E., Stock, C., Hermann, A., Cokelet, E., Mordy, C., Stabeno, P., Hervieux, G., Castruccio, F., 2016. What processes contribute to the spring and fall bloom co-variability on the Eastern Bering Sea shelf? Deep-Sea Res. II. 00, 00-00, this issue.

Ciannelli, L., Brodeur, R. D., Buckley, T. W., 1998. Development and application of a bioenergetics model for juvenile walleye pollock. J. Fish Biol. 52, 879–898.

Coachman, L.K., 1986. Circulation, water masses, and fluxes on the southern Bering Sea shelf. Continental Shelf Res. 5, 23-108.

Coachman, L.K., Aagaard, K., Tripp, R.B., 1975. Bering Strait: the regional physical oceanography. University of Washington Press, Seattle. 172 p.

1028 Coyle, K.O., Eisner, L.B., Mueter, F.J., Pinchuk, A.I., Janout, M.A., Cieciel, K.D., Farley, E.V.,
1029 Andrews, A.G., 2011. Climate change in the southeastern Bering Sea: impacts on pollock
1030 stocks and implications for the oscillating control hypothesis. Fish. Ocean. 20:139–156.
1031 Curchitser, E.N., Haidvogel, D.B., Hermann, A.J., Dobbins, E.L., Powell, T.M., Kaplan, A.,
1032 2005. Multi-scale modeling of the North Pacific Ocean: Assessment and analysis of
1033 simulated basin-scale variability (1996–2003), J. Geophys. Res. 110, C11021,
1034 doi:10.1029/2005JC002902.
1035 Dalpadado, P., Skojdal, H.R., 1996. Abundance, maturity and growth of the krill species
1036 *Thysanoessa inermis* and *T. longicaudata* in the Barents Sea. Mar. Ecol. Prog. Ser. 144:
1037 175-183.
1038 Danielson, S., Curchitser, E., Hedstrom, K., Weingartner, T., Stabeno, P., 2011. On ocean and
1039 sea-ice modes of variability in the Bering Sea. J. Geophys. Res. 116, C12034,
1040 doi:10.1029/2011JC007389.
1041 Danielson, S., Hedstrom, K., Aagaard, K., Weingartner, T., Curchitser, E., 2012. Wind-induced
1042 reorganization of the Bering shelf circulation. Geophys. Res. Lett. 39, L08601,
1043 http://dx.doi.org/10.1029/2012GL051231.
1044 Dean, K.G., McRoy, P., Ahlnäs, K., Springer, A., 1989. The plume of the Yukon River in
1045 relation to the oceanography of the Bering Sea. Remote Sens. Environ. 28, 75-84.
1046 Denlinger, L.M., 2006. Alaska Seabird Information Series. Unpubl. Rept., U.S. Fish and Wildl.
1047 Serv., Migr. Bird Manage. Nongame Program, Anchorage, AK. downloaded 05/2013
1048 http://www.fws.gov/alaska/mbsp/mbm/seabirds/pdf/asis_complete.pdf.
1049 Eisner, L.B., Gann, J.C., Ladd, C., Cieciel, K.D., Mordy, C., This issue. Late summer/early fall
1050 phytoplankton biomass (chlorophyll a) in the eastern Bering Sea: Spatial and temporal
1051 variations and factors affecting chlorophyll a concentrations. Deep-Sea Res. 0, 00-00.
1052 Eisner, L.B., Napp, J.M., Pinchuk, A., Andrews, A., 2014. Climate-mediated changes in
1053 zooplankton community structure for the eastern Bering Sea. Deep-Sea Res. II 109, 157-
1054 171.
1055 Escoffier, N., Bernard, C., Hamlaoui, S., Groleau, A., Catherine, A., 2015. Quantifying plankton
1056 communities using spectral fluorescence: the effects of species composition and
1057 physiological states. J. Plankton Res., 37, 233-247.

1058 Fissel, B., Dalton, M., Felthoven, R., Garber-Yonts, B., Haynie, A., Himes-Cornell, A.,
1059 Kasperski, S., Lee, J., Lew, D., Seung, C., 2015. Economic status of the groundfish
1060 fisheries off Alaska, 2014. In: Stock assessment and fishery evaluation report for the
1061 groundfish resources of the Bering Sea/Aleutian Islands regions. North Pacific Fishery
1062 Management Council, 605 W. 4th Avenue, Suite 306, Anchorage, AK 99501.
1063 Friday, N.A., Waite, J.M., Zerbini, A.N., Moore, S.E., 2012. Cetacean distribution and
1064 abundance in relation to oceanographic domains on the eastern Bering Sea shelf: 1999-
1065 2004. Deep-Sea Res. II 65-70, 260-272.
1066 Friday, N.A., Zerbini, A.N., Waite, J.M., Moore, S.E., Clapham, P.J., 2013. Cetacean
1067 distribution and abundance in relation to oceanographic domains on the eastern Bering Sea
1068 shelf: 2002, 2008 and 2010. Deep-Sea Res. II 94, 244-256.
1069 Fulton, E.A., 2010. Approaches to end-to-end ecosystem models. Jour. Mar. Sys. 81, 171-183.
1070 Fulton, E A., 2011. Interesting times: winners, losers, and system shifts under climate change
1071 around Australia ICES J. Mar. Sci. 68, 1329-1342.
1072 Fulton E.A., Smith, A,D.M, Smith, D.C., Johnson, P., 2014. An Integrated approach is needed
1073 for ecosystem based fisheries management: Insights from ecosystem-level management
1074 strategy evaluation. PLoS ONE 9(1): e84242. doi:10.1371/journal.pone.0084242
1075 Gibson, G.A., Spitz, Y.H., 2011. Impacts of biological parameterization, initial conditions, and
1076 environmental forcing on parameter sensitivity and uncertainty in a marine ecosystem
1077 model for the Bering Sea. J. Mar. Sys. 88, 214-231.
1078 Harvey, M., Galbraith, P.S., Descroix, A., 2009. Vertical distribution and diel migration of
1079 macrozooplankton in the St. Lawrence marine system (Canada) in relation with the cold
1080 intermediate layer thermal properties. Prog. Oceanogr. 80, 1-21.
1081 Harvey, H.R., Pleuthner, R.L., Lessard, E.J., Bernhardt, M.J., Shaw, T.C., 2012. Physical and
1082 biochemical properties of the euphausiids *Thysanoessa inermis*, *Thysanoessa raschii*, and
1083 *Thysanoessa longipes* in the eastern Bering Sea. Deep-Sea Res. II 65-70, 173-183.
1084 Heintz, R.A., Siddon., E.C., Farley Jr., E.C., Napp, J.M., 2013. Correlation between recruitment
1085 and fall condition of age-0 pollock (*Theragra chalcogramma*) from the eastern Bering Sea
1086 under varying climate conditions. Deep-Sea Res. II 94, 150-156.

1087 Hermann, A.J., Gibson, G.A., Bond, N.A., Curchitser, E.N., Hedstrom, K., Cheng, W., Wang,
1088 M., Cokelet, E.D., P.J. Stabeno, Aydin, K., 2016. Projected futures biophysical states of
1089 the Bering Sea. Deep-Sea Res II 00, 00-00, this issue.
1090 Hermann, A. J., Gibson, G.A., Bond, N.A., Curchitser, E.N., Hedstrom, K., Cheng, W., Wang,
1091 M., Stabeno, P.J., Eisner, L. Cieciel, K.D., 2013. A multivariate analysis of observed and
1092 modeled biophysical variability on the Bering Sea shelf: multidecadal hindcasts (1970-
1093 2009) and forecasts (2010-2040). Deep-Sea Res II, 94, 121-139.
1094 doi:10.1016/j.dsr2.2013.04.007.
1095 Hollowed, A.B, Aydin, K.Y., Essington, T.E., Ianelli, J.N., Megrey, B.A., Punt, A.E., Smith,
1096 A.D.M., 2011. Experience with quantitative ecosystem assessment tools in the northeast
1097 Pacific Fish and Fisheries 12, 189-208.
1098 Hollowed, A.B., Barbeaux, S., Farley, E., Cokelet, E.D., Kotwicki, S., Ressler, P.H., Spital, C.,
1099 Wilson, C.D., 2012. Effects of climate variations on pelagic ocean habitats and their role
1100 in structuring forage fish distributions in the Bering Sea. Deep-Sea Res. II, 65-70, 230-
1101 250.
1102 Hollowed, A.B., Curchitser, E.N., Stock, C.A., Zhang, C.I., 2013. Trade-offs associated with
1103 different modeling approaches for assessment of fish and shellfish responses to climate
1104 change. Climatic Change 119, 111-129.
1105 Huenerlage, K., Graeve, M., Buchholz, C., Buchholz, F., 2015. The other krill: overwintering
1106 physiology of adult *Thysanoessa inermis* (Euphausiacea) from the high-Arctic Kongsfjord.
1107 Aquat. Biol. 23, 225-235.
1108 Hunt Jr., G.L., , Allen, B.M., Angliss, R.P., Baker, T., Bond, N., Buck, G., Byrd, G.V., Coyle,
1109 K.O., Devol, A., Eggers, D.M., Eisner, L., Feely, R., Fitzgerald, S., Fritz, L.W. Gritsay,
1110 E.V., Ladd, C., Lewis, W., Mathis, J., Mordy, C.W., Mueter, F., Napp, J., Sherr, E., Shull,
1111 D., Stabeno, P., Stepanenko, M.A., Strom, S., Whitledge, T.E. 2010. Status and trends of
1112 the Bering Sea region, 2003-2008, pp 196-267. In: S.M. McKinnell and M.J. Dagg [Eds.]
1113 Marine Ecosystems of the North Pacific Ocean, 2003-2008. PICES Special Publication 4,
1114 393 p.
1115 Hunt Jr., G.L., Coyle, K.O., Eisner, L.B., Edward V., Heintz, R.A., Mueter, F., Napp, J.M.,
1116 Overland, J.E., Ressler, P.H., Salo, S., Stabeno, P.J., 2011. Climate impacts on eastern

1117 Bering Sea foodwebs: a synthesis of new data and an assessment of the Oscillating Control
1118 Hypothesis. ICES J. Mar. Sci. 68, 1230-1243.
1119 Hunt Jr., G.L., Renner, M., Kuletz, K., 2014. Seasonal variation in the cross-shelf distribution of
1120 seabirds in the southeastern Bering Sea. Deep-Sea Res. II 109, 266-281.
1121 Hunt Jr., G.L., Jr., Ressler, P.H., Gibson, G., DeRobertis, A., Aydin, K., Sigler, M.F., Ortiz, I.,
1122 Lessard, E.J., Williams, B.C., Pinchuk, A.I., Buckley, T., 2016. What controls the
1123 distribution and abundance of euphausiids over the southeastern Bering Sea shelf? Deep-
1124 Sea Res. II 00, 00–00, this issue.
1125 Ianelli, J., Holsman, K.K., Punt, A.E., Aydin, K., 2016. Multi-model inference for incorporating
1126 trophic and climate uncertainty into stock assessments. Deep-Sea Res. II 00, 00–00, this
1127 issue.
1128 Ianelli, J., Honkahleto, T., Barbeaux, S., Kotwicki, S. Aydin, K., Williamson, N., 2011.
1129 Assessment of the walleye pollock stock in the eastern Bering Sea. In: Stock assessment
1130 and fishery evaluation report for the groundfish resources of the Bering Sea/Aleutian
1131 Islands regions. North Pacific Fishery Management Council, 605 W. 4th Avenue, Suite
1132 306, Anchorage, AK 99501.
1133 Iguchi, N., Ikeda, T., 2004. Vertical distribution, population structure and life history of
1134 *Thysanoessa longipes* (Crustacea:Euphausiacea) around Yamato Rise: central Japan. J. of
1135 Plankton Res. 26, 1015-1023.
1136 IPCC. 2007. Climate Change 2007: Working Group I: The Physical Science Basis. Contribution
1137 of Working Group I to the fourth assessment report of the intergovernmental panel on
1138 climate change, 2007. Solomon, S., Qin, D., Manning, M., Chen, Z., Marquis, M., Averyt,
1139 K,B., Tignor, M., Miller, H.L. (Eds.). Cambridge University Press, Cambridge, United
1140 Kindgdom and New York, NY, USA. 996 pp.
1141 IPCC, 2013: Climate Change 2013: The Physical Science Basis. Contribution of Working Group
1142 I to the Fifth Assessment Report of the Intergovernmental Panel on Climate Change
1143 [Stocker, T.F., Qin, D., Plattner, G.K., Tignor, T., Allen, S.K., Boschung, J., Nauels, A.,
1144 Xia, Y., Bex, V., and Midgley, P.M. (eds.)]. Cambridge University Press, Cambridge,
1145 United Kingdom and New York, NY, USA, 1535 pp.

1146 Jurado-Molina, J. Livingston, P.A., Ianelli, J.N., 2005. Incorporating predation interactions in a
1147 statistical catch-at-age model for predator-prey system in the Bering Sea. Can. J. Fish.
1148 Aquat. Sci. 62, 1865-1873.
1149 Kinzey, D., Punt, A.E., 2009. Multispecies and single-species models of fish population
1150 dynamics: comparing parameter estimates. Nat. Resour. Model. 22, 67-104.
1151 Kishi, M.J, Ito, S., Megrey, B.A., Rose, K.A., Werner, F.E., 2011. A review of the NEMURO
1152 and NEMURO.FISH models and their application to marine ecosystem investigations. J.
1153 Ocean. 67, 3-16.
1154 Kishi, M.J., Kashiwai, M., Ware, D.M., Megrey, B.A., Eslinger, D.L., Werner, F.E., Noguchi-
1155 Aita, M., Azumaya, T., Fujii, M., Hashimoto, S., Huang, D., Iizumi, H., Ishida, Y., Kang,
1156 S., Kantakov, G.A., Kim, H-C., Komatsu, K., Navrotsky, V.V., Smith, S.L., Tadokoro, K.,
1157 Tsuda, A., Yamamura, O., Tamanaka, Y., Yokouchi, K., Yoshie, N., Zhang, J., Zuenko,
1158 Y.I., Zvalinsky, V.I., 2007. NEMURO—a lower trophic level model for the North Pacific
1159 marine ecosystem. Ecol. Model. 202,12–25.
1160 Kotwicki, S., Buckley, T., Honkahleto, T., Walters, G., 2005. Variation in the distribution of
1161 walleye pollock (*Theragra chalcogramma*) with temperature and implications for seasonal
1162 migration. Fish. Bull. 103, 574-587.
1163 Kotwicki, S., Horne, J.K., Punt, A.E., Ianelli, J.N., 2015. Factors affecting the availability of
1164 walleye pollock to acoustic and bottom trawl survey gear. ICES J. Mar. Sci. 72, 1425-
1165 1439.
1166 Lauth, R., Kotwicki, S., 2013. Detecting temporal trends and environmentally-driven changes in
1167 the spatial distribution of bottom fishes and crabs in the eastern Bering Sea shelf. Deep-Sea
1168 Res. II 94, 231-243.
1169 Large W.G., Yeager, S.G., 2009. The global climatology of an interannually varying air-sea
1170 1009 flux data set. Clim. Dyn., 33, 341-364.
1171 Livingston, P.A., Aydin, K., Boldt, J., Ianelli, J., Jurado-Molina, J., 2005. A framework for
1172 ecosystem impacts assessment using an indicator approach. ICES J. Mar. Sci. 62, 592-597.
1173 Livingston, P.A., Methot, R.D., 1998. Incorporation of predation into a population assessment
1174 model of eastern Bering Sea walleye pollock. P. 663-678. In: Fishery Stock Assessment
1175 Models. Alaska Sea Grant College Program Publication AK-SG-98-01. 1037p.

1176 Lomas, M.W., Moran, S.B., Casey, J.R., Bell, D.W., Tiahlo, Whitefield, J., Kelly, R.P., Mathis,
1177 J.T., Cokelet, E.D., 2012. Spatial and seasonal variability of primary production on the
1178 eastern Bering Sea shelf. Deep-Sea Res. II, 65-70, 126-140.
1179 Luchin, V., Panteleev, G., 2014. Thermal regimes of the Chukchi Sea from 1941 to 2008. Deep-
1180 Sea Res. II 109, 14–26.
1181 Moffitt, E., Punt, A.E., Holsman, K., Aydin, K.Y., Ianelli, J.N., Ortiz, I. 2016. Moving towards
1182 Ecosystem-Based Fisheries Management: options for parametrizing multi-species
1183 biological reference points. Deep-Sea Res. II. 00, 00-00, this issue.
1184 Morata, N, Søreide, J.E., 2015. Effect of light and food on the metabolism of the Arctic copepod
1185 *Calanus glacialis*. Polar Biol. 38, 67-73.
1186 Mordy, C.W, Eisner, L.B., Proctor, P., Stabeno, P., Devol, A.H., Shull, D.H., Napp, J.M.,
1187 Whitledge, T. 2010. Temporary uncoupling of the marine nitrogen cycle: Accumulation of
1188 nitrite on the Bering Sea shelf. Marine Chemistry, 121, 157-166.
1189 Mueter, F.J. and M.A. Litzow. 2008. Sea ice retreat alters the biogeography of the Bering Sea
1190 continental shelf. Ecological Applications, 18, 309-320.
1191 Niebauer, H.J., Alexander, V., Henrich, S.M., 1995. A time-series study of the spring bloom at
1192 the Bering Sea-ice edge I: physical processes, chlorophyll and nutrient chemistry.
1193 Continental Shelf Res. 15, 1859–1877.
1194 North Pacific Fishery Management Council (NPFMC). 2009. Stock assessment and fishery
1195 evaluation report for the groundfish fisheries of the Gulf of Alaska and Bering
1196 Sea/Aleutian Islands area: Economic status of the Groundfish fisheries off Alaska, 2012.
1197 North Pacific Fishery Management Council 605 West 4th Ave., Suite 306 Anchorage, AK
1198 99501
1199 North Pacific Fishery Management Council (NPFMC). 2014. Stock assessment and fishery
1200 evaluation report for the groundfish fisheries of the Gulf of Alaska and Bering
1201 Sea/Aleutian Islands area: Economic status of the Groundfish fisheries off Alaska, 2012.
1202 North Pacific Fishery Management Council 605 West 4th Ave., Suite 306 Anchorage, AK
1203 99501.
1204 Orlova, E.M., Dolgov, A.V., Renaud, P.E., Greenacre, M., Halsband, C., Ivshin, V.A., 2014.
1205 Climatic and ecological drivers of euphausiid community structure vary spatially in the

1206 Barents Sea: relationships from a long time series (1952-2009). Front. Mar. Sci. 1: 1–13.
1207 doi: 10.3389/fmars.2014.00074.
1208 Ortiz, I., Wiese, F. K., Grieg, A., 2012. Marine Regions Boundary Data for the Bering Sea Shelf
1209 and Slope. UCAR/NCAR-Earth Observing Laboratory/Computing, Data, and Software
1210 Facility. Dataset. http://dx.doi.org/10.5065/D6DF6P6C
1211 Overland. J.E, Salo, S.A., Kantha, L. H., Clayson, C.A., 1999. Thermal stratification and mixing
1212 in the Bering Sea shelf. pp.129-215. In: Loughlin, T.R., Ohtani, K., (Eds.) 1999. Dynamics
1213 of the Bering Sea. University of Alaska Sea Grant, AK-SG-99-03, Fairbanks, 838 p.
1214 Page, L.M., Espinosa-Pérez, H., Findley, L.T., Gilbert, C.R., Lea, R.N., Mandrak, N.E., Mayden,
1215 R.L., Nelson, J.S., 2013. Common and scientific names of fishes from the United States,
1216 Canada, and Mexico, 7th edn. Spec. Publ. Am. Fish. Soc. No. 34, Bethesda, MD. 243 pp.
1217 Petrik, C.M., Duffy-Anderson, J.T., Mueter, F., Hedstrom, K., Curchitser, E.N., 2015.
1218 Biophysical transport model suggests climate variability determines distribution of
1219 Walleye Pollock early life stages in the eastern Bering Sea through effects on spawning.
1220 Prog. Oceanogr. 138, 459-474.
1221 Punt, A.E., Ortiz, I., Aydin, K.Y., Hunt Jr. G.L., Wiese, F.K., 2016. End-to-End modeling as part
1222 of an Integrated Research Program in the Bering Sea. Deep-Sea Res. II. 00, 00-00, this
1223 issue.
1224 Ressler, P.H., De Robertis, A, Kotwicki, S., 2014. The spatial distribution of euphausiids and
1225 walleye pollock in the eastern Bering Sea does not imply top-down control by predation.
1226 Mar. Ecol. Prog. Ser. 503, 111-222.
1227 Ressler, P.H., De Robertis, A, Warren, J.D., Smith, J.N., Kotwicki, S., 2012. Developing an
1228 acoustic survey of euphausiids to understand trophic interactions in the Bering Sea
1229 ecosystem. Deep-Sea Res. II, 65-70, 184-195.
1230 Rho, T., Whitledge, T.E., 2007. Characteristics of seasonal and spatial variations of primary
1231 production over the southeastern Bering Sea shelf. Continental Shelf Res. 27, 2556–2569.
1232 Rose, K.A., Allen, J.I., Artioli, Y., Barange, M., Blackford, J., Carlotti, F., Cropp, R., Daewell,
1233 U., Edwards, K., Flynn, K., Hill, S,L., HilleRisLambers, R., Huse, G., Mackinson, S.,
1234 Megrey, B., Moll, A,. Rivkin, R., Salihoglu, B., Schrum, C., Shannon, L., Shin, Y., Smith,
1235 S.L., Smith, C., Solidoro, C., St. John, M., Zhou, M., 2010. End-to-End modeling for the

1236 analysis of marine ecosystems: challenges, issues and next steps. Mar. Coast. Fish. 2, 115–
1237 130.
1238 Rose, K.A. Fiechter, J., Curchitser, E. N., Hedstrom, K., Bernal, M., Creekmore, S., Haynie, A.,
1239 Ito, S., Lluch-Cota, S., Megrey, B.A., Edwards, C.A., Checkley, D., Koslow, T.,
1240 McClatchie, S., Werner, F., MacCall, A., Agostini, V., 2015. Demonstration of a fully-
1241 coupled end-to-end model for small pelagic fish using sardine and anchovy in the
1242 California Current. Prog. Oceanogr. 138, 348-380.
1243 Russel, R.W., Harrison, N.M., Hunt Jr., G.L., 1999. Foraging at a front: hydrography ,
1244 zooplankton and avian planktivory in the northern Bering Sea, Mar. Ecol. Prog. Ser. 182,
1245 77-93.
1246 Saha, S. Moorthi, S., Pan, H.-L., Wu, X., Wang, J., Nadiga, S., Tripp, P., Kistler, R., Woollen J.,
1247 Behringer, D., Liu, H., Stokes, D., Grumbine, R., Gayno, G., Wang, J., Hou, Y.-T.,
1248 Chuang, H-Y., Juang, H.-M. H., Sela, J., Iredell, M., Treadon, R., Kleist, D., Van Delst, P.,
1249 Keyser, D., Derber, J., Ek, M., Meng, J., Wei, H., Yang, R., Lord, S., Van Den Dool, H.,
1250 Kumar, A., Wang, W., Long, C., Chelliah, M., Xue, Y., Hunag, B., Schemm, J.-K.,
1251 Ebisuzaki, W., C.-Z., Liu, Q., Chen, Y., Han, Y., Cucurull, L., Reynolds, R.W., Rutledge,
1252 G., Goldberg, M., 2010. The NCEP Climate Forecast System Reanalysis. Bull. Amer. 873
1253 Meteor. Soc. 91, 1015-1057 http://dx.doi.org/10.1175/2010BAMS3001.1
1254 Salinger, M.J., 2013. A brief introduction to the issue of climate and marine fisheries. Climatic
1255 Change 119, 23-35.
1256 Salomone, P., Morstad, S., Sands, T., Jones, M., Baker, T., Buck, G., West, F., Kerig, T., 2011.
1257 2010 Bristol Bay Area Annual Management Report. Fishery Management Report No. 11-
1258 23. http://www.adfg.alaska.gov/FedAidpdfs/FMR11-23.pdf
1259 Sargent, J.R., Falk-Petersen, S., 1981. Ecological investigations on the zooplankton community
1260 in Balsfjorden, northern Norway: lipids and fatty acids in *Meganyctiphanes norvegica*,
1261 *Thysanoessa raschi* and *T. inermis* during midwinter.Mar Biol 62, 131–137.
1262 Siddon, E.C., Kristiansen, T., Mueter, F.J., Holsman, K.K., Heintz, R.A., Farley, E.V., 2013.
1263 Spatial match-mismatch between juvenile fish and prey provides a mechanism for
1264 recruitment variability across contrasting climate conditions in the eastern Bering Sea.
1265 PLoS ONE 8(12): e84526. doi:10.1371/journal.pone.0084526

1266 Sigler, M.F., Stabeno, P.J., Eisner, L.B., Napp, J.M., Mueter, F.J., 2014. Spring and fall
1267 phytoplankton blooms in a productive subarctic ecosystem, the eastern Bering Sea, during
1268 1995-2011. Deep-Sea Res. II, 109, 71-83.
1269 Smith, S.L., 1991. Growth, development and distribution of the euphausiids *Thysanoessa raschii*
1270 (M. Sars) and *Thysanoessa inermis* (Krøyer) in the southeastern Bering Sea. Polar Res. 10,
1271 461–478.
1272 Stabeno, P.J., Bond, N.A., Salo, S.A., 2007. On the recent warming of the southeastern Bering
1273 Sea shelf. Deep-Sea Res. II, 54, 2599-2618.
1274 Stabeno, P.J., Danielson, S., Kachel, N.B., Mordy, C.W., 2016. Currents on eastern Bering Sea
1275 shelf, Deep-Sea Res. II 00, 00-00, this issue.
1276 Stabeno, P. J., Hunt Jr, G.L., 2002. Overview of the inner front and southeast Bering Sea
1277 carrying capacity programs. Deep-Sea Res. II, 49, 6157-6168.
1278 Stabeno, P.J., Farley Jr, E.V., Kachel, N.B., Moore, S., Mordy, C.W., Napp, J.M., Overland, J.E.,
1279 Pinchuk, A.I., Sigler, M.F., 2012a. A comparison of the physics of the northern and
1280 southern shelves of the eastern Bering Sea and some implications for the ecosystem. Deep-
1281 Sea Res. II. 65, 14-30.
1282 Stabeno, P.J., Kachel, N.B., Moore, S.E., Napp, J.M., Sigler, M., Yamaguchi, A., Zerbini, A.N.,
1283 2012b. Comparison of warm and cold years on the southeastern Bering Sea shelf and some
1284 implications for the ecosystem. Deep-Sea Res. II. 65, 31-45.
1285 Stabeno, P., Napp, J., Mordy, C., Whitledge, T., 2010. Factors influencing physical structure and
1286 lower trophic levels of the eastern Bering Sea shelf in 2005: Sea-ice, tides and winds. Prog.
1287 Oceanogr. 85, 80-196.
1288 Stabeno, P.J., Schumacher, J.D., Davis, R. F., Napp, J. M., 1998. Under-ice observations of
1289 water column temperature, salinity and spring phytoplankton dynamics: eastern Bering Sea
1290 shelf. J. Mar. Res. 56, 239–255.
1291 Sullivan, M.E., Kachel, N.B., Mordy, C.W., Salo, S.A., Stabeno, P.J., 2014. Sea-ice and water
1292 column structure on the eastern Bering Sea shelf. Deep-Sea Res. II 109, 39-56.
1293 Travers, M., Shin, Y.J.; Jennings, S., Cury, P., 2007. Towards end-to-end models for
1294 investigating the effects of climate and fishing in marine ecosystems Prog. Oceanogr. 75,
1295 751-770.

1296 Travers, M., Shin, Y J., Jennings, S., Machu, E., Huggett, J.A., Field, J.G., Cury, P.M., 2009.
1297 Two-way coupling versus one-way forcing of plankton and fish models to predict
1298 ecosystem changes in the Benguela. Ecol. Model. 220, 3089-3099.
1299 Travers-Trolet, M, Shin, Y-J, Field, J.G., 2014a. An end-to-end coupled model ROMS-
1300 N2P2Z2D2-OSMOSE of the southern Benguela foodweb: parameterisation, calibration
1301 and pattern-oriented validation. Afr. J. Mar. Sci. 36, 11-29.
1302 Travers-Trolet, M., Shin, Y-J., Shannon, L.J., Moloney, C.L., Field, J.G. 2014b. Combined
1303 Fishing and Climate Forcing in the Southern Benguela Upwelling Ecosystem: An End-to-
1304 End Modelling Approach Reveals Dampened Effects. PLoS One 9, E94286.
1305 Tsuda, A., Saito, H., Kasai, H., 2001. Life history strategies of subarctic copepods *Neocalanus*
1306 *flemingeri* and *N. plumchrus*, especially concerning lipid accumulation patterns. Plankton
1307 Biol. Ecol. 48, 52-58.
1308 Vidal, J., Smith, S.L., 1986. Biomass, growth, and development of populations of herbivorous
1309 zooplankton in the southeastern Bering Sea during spring. Deep-Sea Res. II. 33, 523–556.
1310 Ware, D.M.,1978. Bioenergetics of pelagic fish: theoretical change in swimming speed and
1311 ration with body size. J. Fish. Res. Board Can. 35, 220–28.
1312 Wang, J., Hu, H., Mizobata, K., Saito, S.-I., 2009. Seasonal variations of sea-ice and ocean
1313 circulation in the Bering Sea: a model-data fusion study. J. Geophys. Res. 114, C02011,
1314 doi:10.1029/2008JC004727.
1315 Wiese, F.K., Wiseman, Jr., W.J., Van Pelt, T.I., 2012. Bering Sea Linkages. Deep-Sea Res. II.
1316 65-70, 2-5.
1317 Witherell, D., Pautzke, C.P., Fluharty, D. 2000. An ecosystem-based approach for Alaska
1318 groundfish fisheries. ICES J. Mar. Sci. 57, 771-777.
1319 Wyllie-Echeverria, T., Wooster, W.S., 1998. Year-to-year variations in Bering Sea-ice cover
1320 and some consequences for fish distributions. Fish. Oceanogr. 7, 1063-1074.
1321 Zador, S. (Ed). 2015. Ecosystem consideration 2015. North Pacific Fishery Management Council
1322 605 West 4th Ave., Suite 306 Anchorage, AK 99501. 297p.
1323 https://www.afsc.noaa.gov.REFM/Docs/2015/ecosystem.pdf
1324

Table 1. List of groups in and their population structure assumed in the FEAST model.
M=mortality, G=growth, R=recruitment, Mov=movement

Group name	Species	No. Age classes	No. Length classes	Length interval (cm)	Processes explicitly modelled
Pollock age-1 and older	*Gadus chalcogrammus*	10	14	4	M, G, R, Mov
Pollock age-0		1	20	2	M, G, R, Mov
Pacific cod age-1 and older	*Gadus macrocephalus*	10	14	4	M, G, R, Mov
Pacific cod age-0		1	20	2	M, G, R, Mov
Arrowtooth flounder age-1 and older	*Atherestes stomias*	10	14	4	M, G, R, Mov
Arrowtooth flounder age-0		1	20	2	M, G, R, Mov
Pacific herring	*Clupea palassi*	-	20	2	Mov
Capelin	*Mallotus villosus*	-	20	2	Mov
Eulachon	*Thaleictes pacificus*	-	20	2	Mov
Pacific Sandlance	*Ammodytes hexapterus*	-	20	2	Mov
Myctophid	*Myctophidae*	-	20	2	-
Squid	*Order Teuthida*	-	fixed at 10		-
Crabs	*Chionecetes opilio*	-	fixed at 2		-
Shrimp	*Pandalidae*	-	fixed at 2		-
Epifauna		-	fixed at 1		-
Misc. zoop.		-	fixed at 2		-

Table 2. Data used for fish initial conditions. RACE= Resource Assessment and Conservation Engineering Division of the Alaska Fisheries Science Center (AFSC); AGP= Age and Growth Program of the AFSC; BTS=Bottom Trawl Survey; BASIS=Bering-Aleutian Salmon International Survey; q is the catchability coefficient as estimated for given species/group from BTS estimates and biomass as estimated by the mass balanced model for the eastern Bering Sea, Aydin et al, 2007)

Group	Numbers/ Biomass	Spatial distribution	Length
Pollock	Stock assessment estimate for 1971 (NPFMC, 2009) plus 2% assumed to inhabit the Northern Bering Sea (based on survey ratio between north and south strata)	RACE mean average year	Length-at-age data from RACE AGP, BTS and BASIS
Cod	Stock assessment estimate for 1971 (NPFMC, 2009)	RACE mean average year	Length-at-age data from RACE AGP, BTS and BASIS
Arrowtooth flounder	Back calculation of numbers-at-age from the stock assessment estimate for 1982 (NPFMC, 2009) less 17% outside the Bering Sea shelf and slope.	RACE mean average year	Length-at-age data from RACE AGP, BTS and BASIS
Herring	Back calculation of numbers-at-age from the stock assessment estimate for 1982 stock assessment (Salomone, 2011)	RACE mean average year	Length at age data from RACE survey
Capelin	Survey estimate in biomass for 1982 *q from Ecopath converted to numbers of fish using a length-weight relationship and assuming population at equilibrium	RACE mean average year	Length data from RACE survey
Eulachon	Survey estimate in numbers for 1982*q from Ecopath	RACE mean average year	Length data from RACE survey
Sandlance	Survey estimate in numbers for 1982*q from Ecopath	RACE mean average year	Length data from RACE survey
Myctophids	Ecopath biomass estimate converted to numbers of fish using a length-weight relationship and assuming the population is at equilibrium	RACE mean average on shelf; uniform distribution off-shelf	Weight at length data from RACE BTS and slope survey
Squid	Ecopath biomass estimate from Aydin et al. (2007)	RACE mean average on shelf + uniform distribution off- shelf	RACE BTS and slope survey
Shrimp	Survey estimate in biomass for 1982*q from Ecopath	RACE mean average year	Length data from RACE BTS
Crab	Survey estimate in biomass for 1982*q from Ecopath	RACE mean average year	Length data from RACE BTS
Epifauna	Survey estimate in biomass for 1982*q from Ecopath	RACE mean average year	Length data from RACE BTS

Figure 1. Data flow and feedbacks across the components of the coupled physical-biological-fish model, Bering10K ROMS-NPZ-FEAST for the Bering Sea. The model has a spatial resolution of ~10 km and 10 vertical layers. Lower trophic levels include an ice module, nutrients, phytoplankton, zooplankton and benthos; fish include 15 species with the three main species being walleye pollock, Pacific cod and arrowtooth flounder; fishing effort is based on historical catches of 16 fisheries defined by sector, gear, and species.

Figure 2. Marine regions used for spatial averaging of results (from Ortiz et al., 2012). Asterisks show Moorings M2, M4, M5 and M8, which are located along the 70m isobath. Insert map shows extent of the Bering10K-ROMS-NPZ-FEAST model.

Figure 3. Nutrient-Phytoplankton-Zooplankton model for the Bering Sea (BESTNPZ, based on Gibson and Spitz, 2011).

Figure 4. Trophic structure and coupled processes represented in the Bering10K-ROMS-BESTNPZ-FEAST model. Note not all fish groups have the same level of modeling detail.

Figure 5. Weekly climatology of ice cover averaged over a 100 km x 100 km box around the four mooring sites (M2, M4, M5 and M8). The Bering10K-ROMS-NPZ-FEAST model simulation (grey line) and satellite observations (thin black) were computed over years 1996 – 2009.

Figure 6. Top 2 rows: annual time series of weekly mean observed chlorophyll-*a* (Chl*a*, mgC/m^3) at 10 m (pink) versus model phytoplankton (grey; large + small) biomass (gC/m^2) at moorings M2, M4, M5, M8. Bottom 2 rows: weekly climatologies of observed chlorophyll-*a* at 10 m (Chl*a*, mgC/m^3) (pink, note change in scale) versus model primary producers biomass (gC/m^2) (black - ice algae; dark grey - large phytoplankton; light grey - small phytoplankton) at moorings M2, M4, M5, M8. Time series and weekly climatologies were computed from 1996 to 2009; no observations were available for moorings M5 and M8 prior to 2004.

Figure 7. Scatterplot of timing of spring bloom maximum (Julian week) and timing of ice retreat (Julian week when ice cover fell below 15%) from observed data for Chl*a* (Sigler et al., 2014) (1^{st} row) and as estimated by the Bering10K-ROMS-BESTNPZ-FEAST model for the period 1996-2009: ice algae only (row 2), large phytoplankton biomass only (row 3), ice algae+large phytoplankton (row 4), large+small phytoplankton biomass (bottom row). Ice algae is the only variable to respond to timing of ice retreat at each mooring site and is overridden by large phytoplankton.

Figure 8. Time series of number of pollock age-1 and older (1971-2009) as estimated in the EBS stock assessment model (black, SAFE) and projected using the FEAST model (grey). Number of age-1 fish calculated by FEAST were corrected to those estimated by the stock assessment at the beginning of every year.

Figure 9. Modeled zooplankton biomass in shelf areas with 2 to 6°C bottom temperature range with weekly values from 1971-2009 for small copepods (top), large copepods (center), and euphausiids (bottom). Black lines show biomass as modeled by the BERING10K-ROMS-BESTNPZ model where zooplankton total mortality is based on a quadratic function resulting in

mortality proportional to biomass. Light gray lines show biomass as modeled by the BERING10K-ROMS-BESTNPZ-FEAST model where zooplankton total mortality is due to both fish predation as calculated by the FEAST model and "other natural zooplankton mortality" (a reduced quadratic mortality function). Note scale for euphausiids is different.

Figure 10. Modeled physical characteristics across Bering Sea shelf and slope: Top row: weekly length of day in hours, N-S variation at 62°N, 58°N and 54°N; second row: weekly climatology of proportion of ice cover; and third row: weekly climatology of integrated temperature in °C (depth averaged temperature). Results shown for selected regions located along the cross-shelf gradient (from left to right: off-shelf, outer, middle and inner shelf) and latitudinal gradient (south, central and northern; number indicates region). Model results are averages over years 1971-2009.

Figure 11. Primary producers and microzooplankton across Bering Sea shelf and slope: Plots show weekly climatology of daily total biomass (gC/m^2) in the water column (max. 300m depth), at selected regions located along a cross-shelf gradient (from left to right: off-shelf, outer, middle and inner shelf) and latitudinal gradient (south (blue), central (purple) and northern (pink)); number indicates region. Top row: ice algae; second row: large phytoplankton; third row: small phytoplankton; and bottom row: microzooplankton. Model results are computed over years 1971-2009. Note ice algae and microzooplankton have different scales. Model results are averages over years 1971-2009.

Figure 12. Secondary producers across Bering Sea shelf and slope: Plots show weekly climatology of daily total biomass (gC/m^2) in water column (max. 300 m depth), at selected regions located along the cross-shelf gradient (from left to right: off-shelf, outer, middle and inner shelf) and latitudinal gradient (south (blue), central (purple) and northern (pink)); number indicates region. Top row: small copepods; second row: large shelf copepods; third row: large oceanic copepods, and bottom row: euphausiids. Model results are averages over years 1971-2009.

Figure 13. Weekly anomalies of euphausiid biomass (mgCm2, bars) and depth-averaged temperature anomaly (red line) at selected regions from 1971-2009. Top to bottom: inner, middle, outer and off-shelf; north (upper) and south (lower) regions are shown for each shelf domain. See section 3.2.4 for details.

Figure 14. Copepods, euphausiids and pollock in pollock stomachs: Plots show monthly frequency of occurrence (first column), and seasonal percent weight in diet by length of fish in cm (columns 2-5) for copepods (dark grey), euphausiids (light grey) and pollock (green). Results are shown for stomachs collected at selected regions: Top row region 1 (north of AK peninsula), region 3 (middle south shelf), region 4 (south outer shelf) and region 8 (north outer shelf). Stomachs were collected year-round, on surveys and by observers, between 1982 and 2013. BSIERP domains 1, 3, 4, and 8 have 31 years of pollock diet data. Samples include all non-empty pollock stomachs.

Figure 15. Seasonal synthesis of physical and biological processes in the eastern Bering Sea shelf and slope.

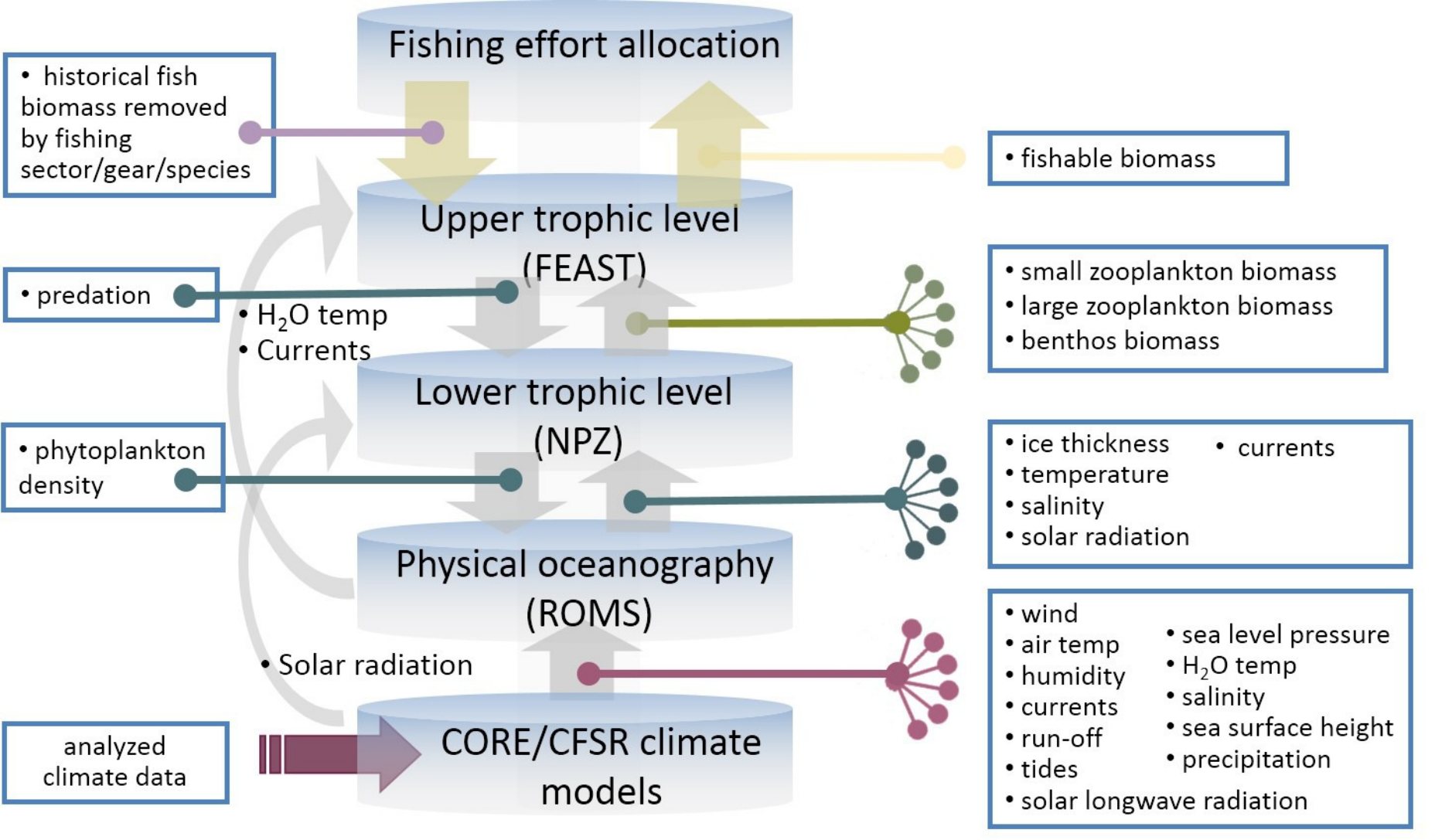
Fishing effort allocation
• historical fish biomass removed by fishing sector/gear/species
• fishable biomass
Upper trophic level (FEAST)
• predation
• H_2O temp
• Currents
• small zooplankton biomass
• large zooplankton biomass
• benthos biomass
Lower trophic level (NPZ)
• phytoplankton density
• ice thickness
• temperature
• salinity
• solar radiation
• currents
Physical oceanography (ROMS)
• Solar radiation
• wind
• air temp
• humidity
• currents
• run-off
• tides
• sea level pressure
• H_2O temp
• salinity
• sea surface height
• precipitation
• solar longwave radiation
analyzed climate data
CORE/CFSR climate models


175°E
180°
175°W
170°W
165°W
160°W
64°N
62°N
60°N
58°N
56°N
54°N
52°N
50°N
68°N
66°N
64°N
62°N
60°N
58°N
56°N
54°N
52°N
13 South Bering Strait
14 Norton Sound
12 St Lawrence
*M8
10 North Middle Shelf
8 North Outer Shelf
9 St Matthew
11 North Inner Shelf
ALASKA
*M5
7 Midnorth Inner Shelf
15 Off-Shelf North
6 Midnorth Middle Shelf
*M4
2 South Inner Shelf
5 Pribilof
3 South Middle *M2 Shelf
4 South Outer Shelf
16 Off-Shelf Southeast
1 AK Peninsula
U.S. Shelf Bathymetry
-200m
-100m
-50m
175°W
170°W
165°W
160°W

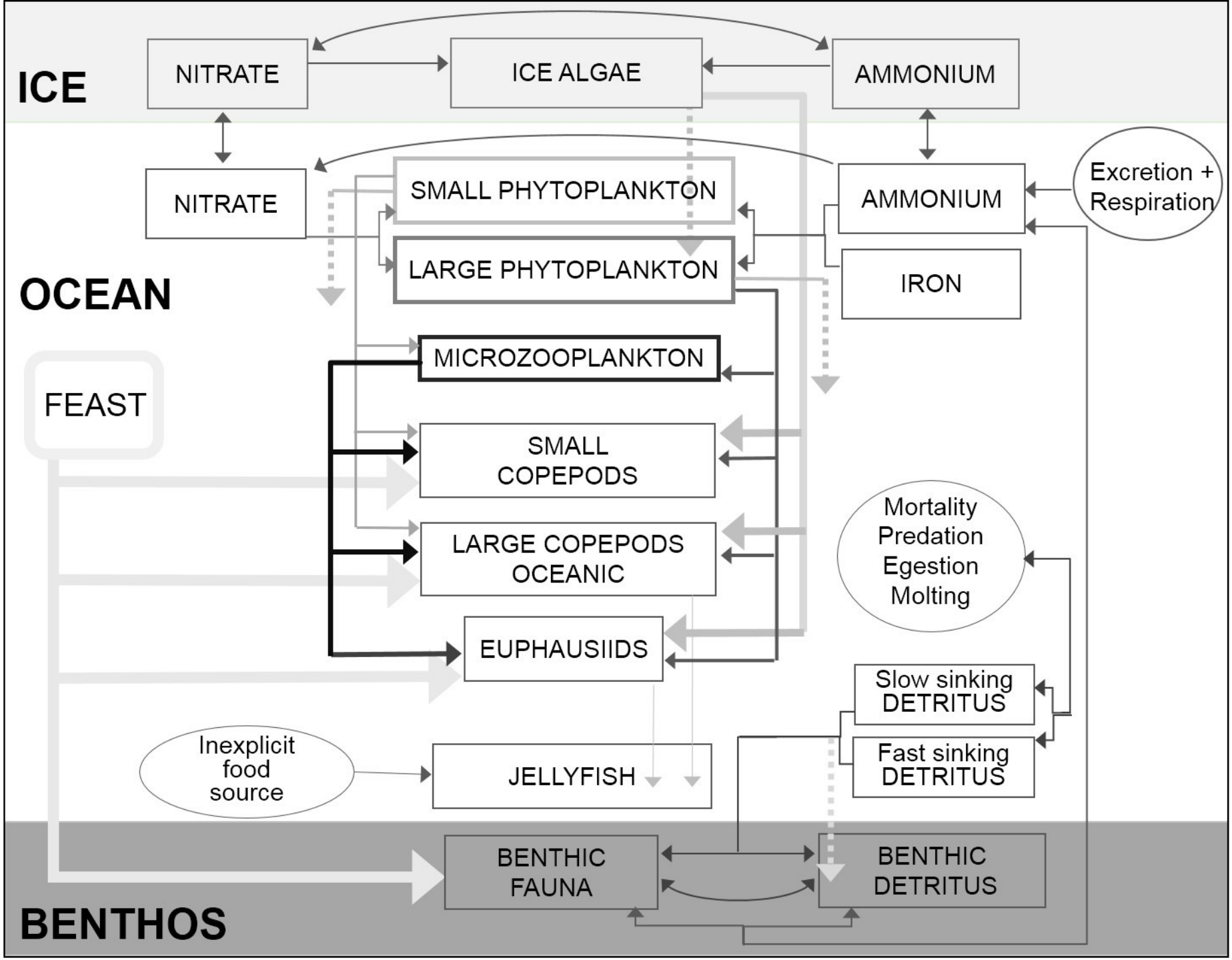
ICE
NITRATE
ICE ALGAE
AMMONIUM
NITRATE
SMALL PHYTOPLANKTON
AMMONIUM
Excretion +
Respiration
OCEAN
LARGE PHYTOPLANKTON
IRON
MICROZOOPLANKTON
FEAST
SMALL
COPEPODS
Mortality
Predation
Egestion
Molting
LARGE COPEPODS
OCEANIC
EUPHAUSIIDS
Slow sinking
DETRITUS
Fast sinking
DETRITUS
Inexplicit
food
source
JELLYFISH
BENTHIC
FAUNA
BENTHIC
DETRITUS
BENTHOS

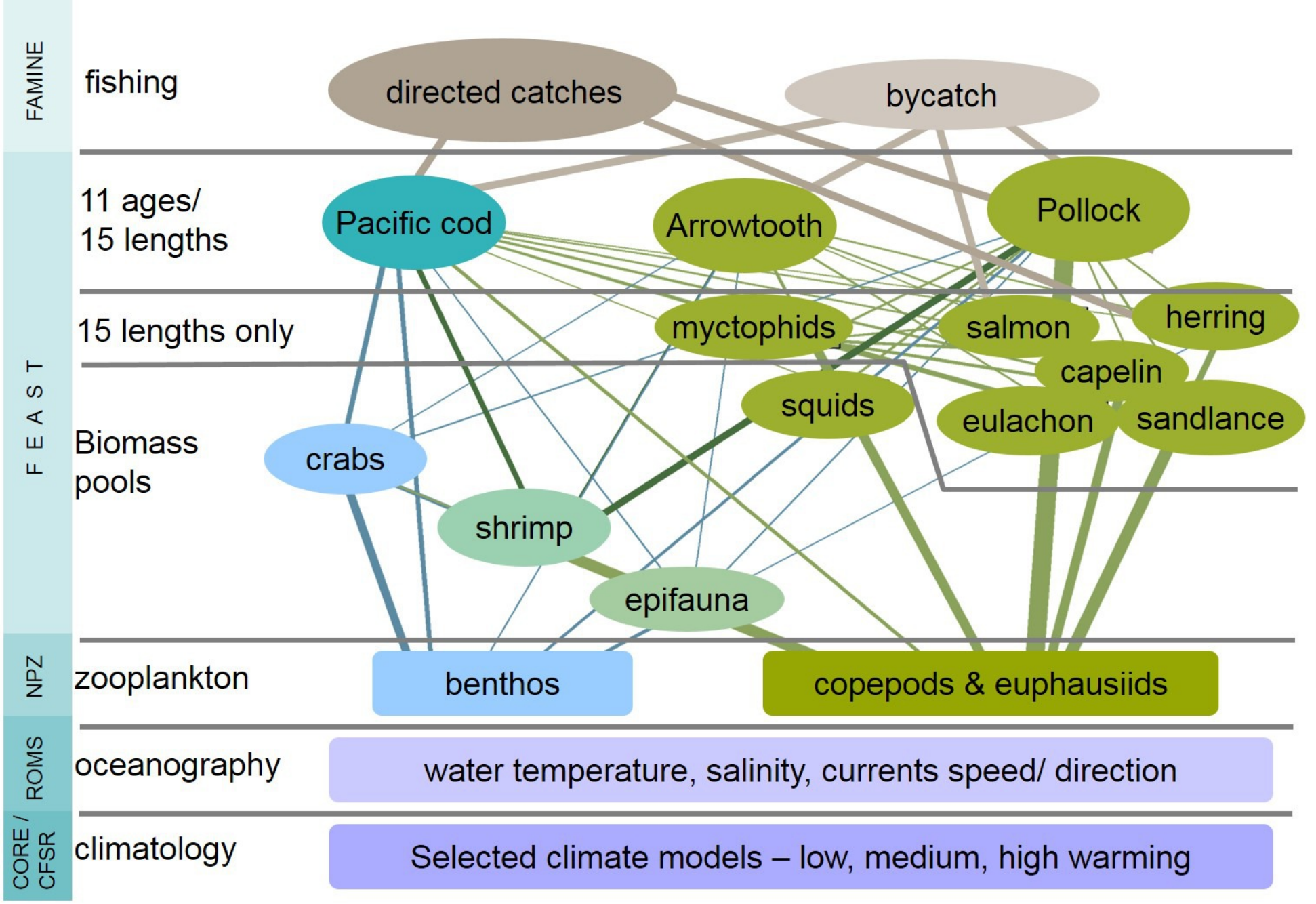
FAMINE
fishing
directed catches
bycatch
FEAST
11 ages/
15 lengths
Pacific cod
Arrowtooth
Pollock
15 lengths only
myctophids
salmon
herring
capelin
squids
eulachon
sandlance
Biomass
pools
crabs
shrimp
epifauna
NPZ
zooplankton
benthos
copepods & euphausiids
ROMS
oceanography
water temperature, salinity, currents speed/ direction
CORE / CFSR
climatology
Selected climate models – low, medium, high warming

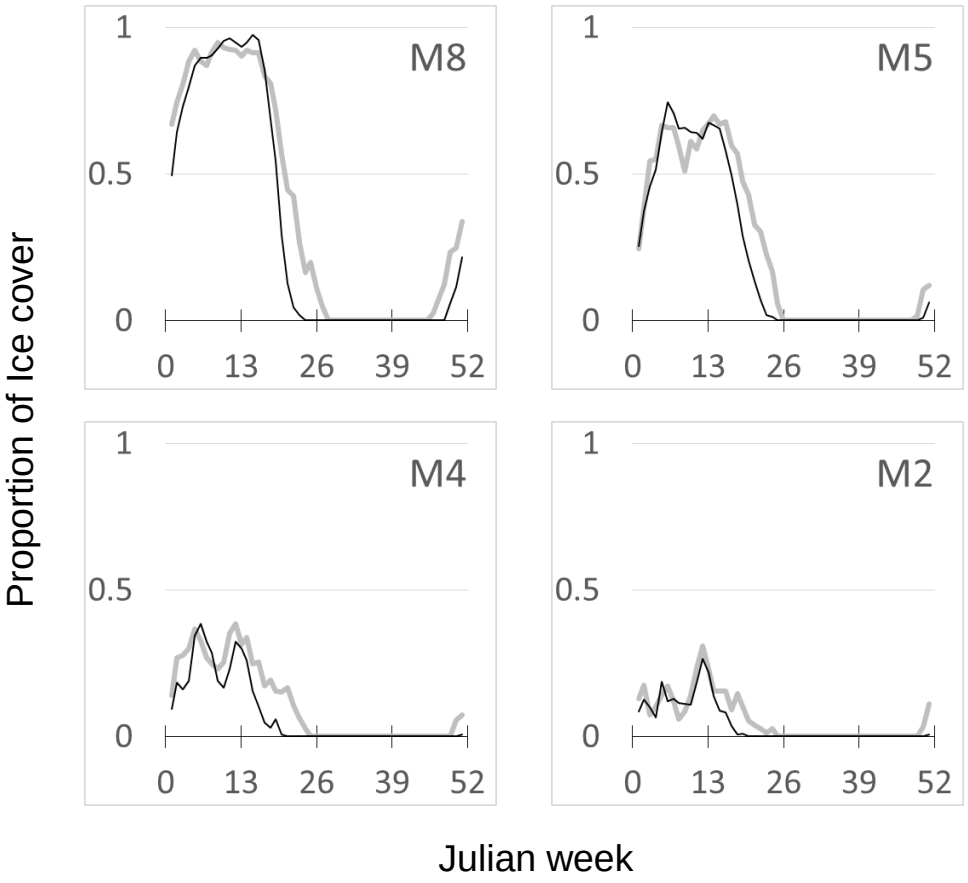
Proportion of Ice cover
M8
M5
M4
M2
1
0.5
0
0
13
26
39
52
Julian week

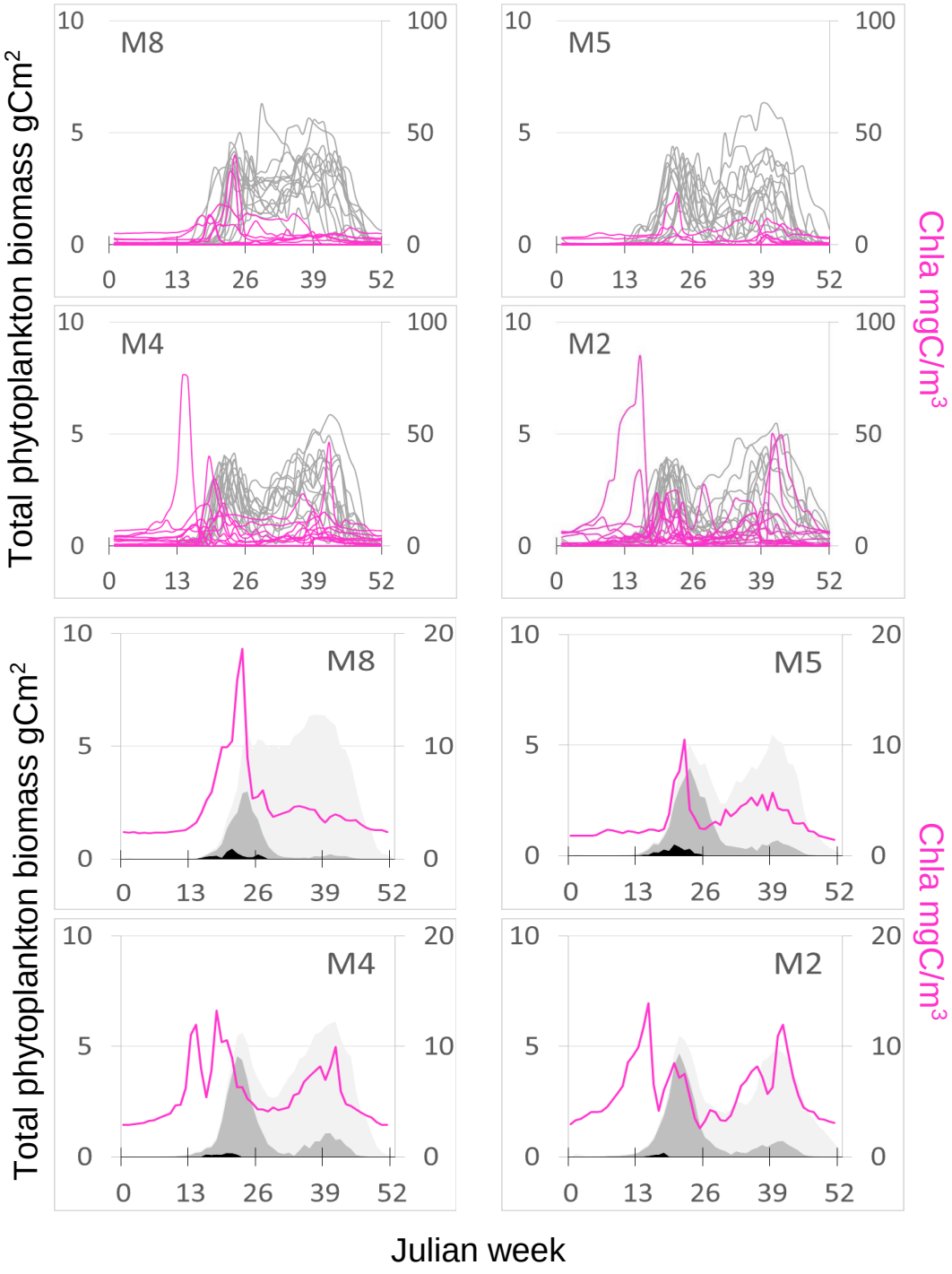
Total phytoplankton biomass gCm²
M8
M5
M4
M2
Chla mgC/m³
Julian week

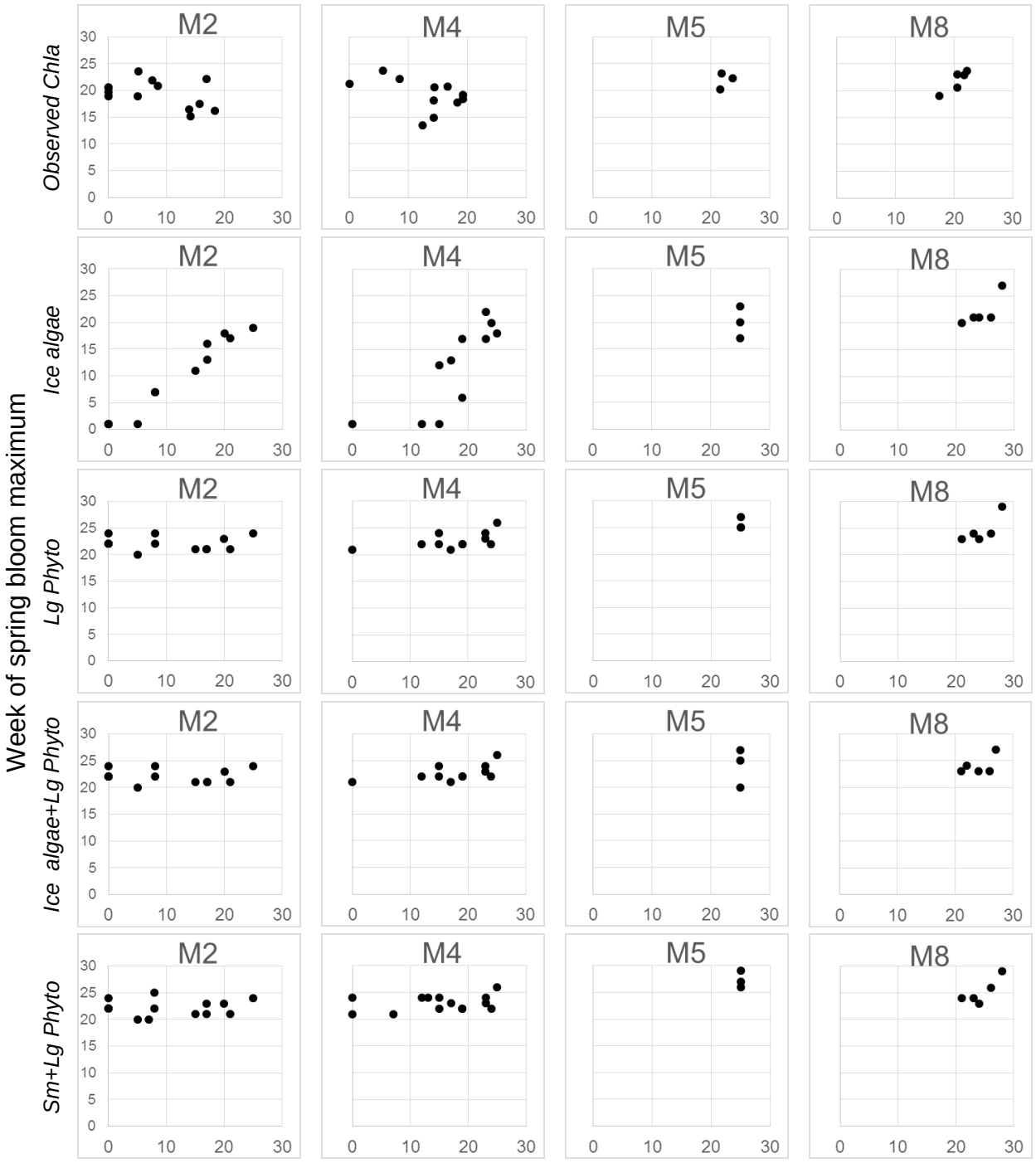
Observed Chla
Ice algae
Lg Phyto
Ice algae+Lg Phyto
Sm+Lg Phyto
M2
M4
M5
M8
Week of spring bloom maximum
Week of ice retreat (15% ice cover)

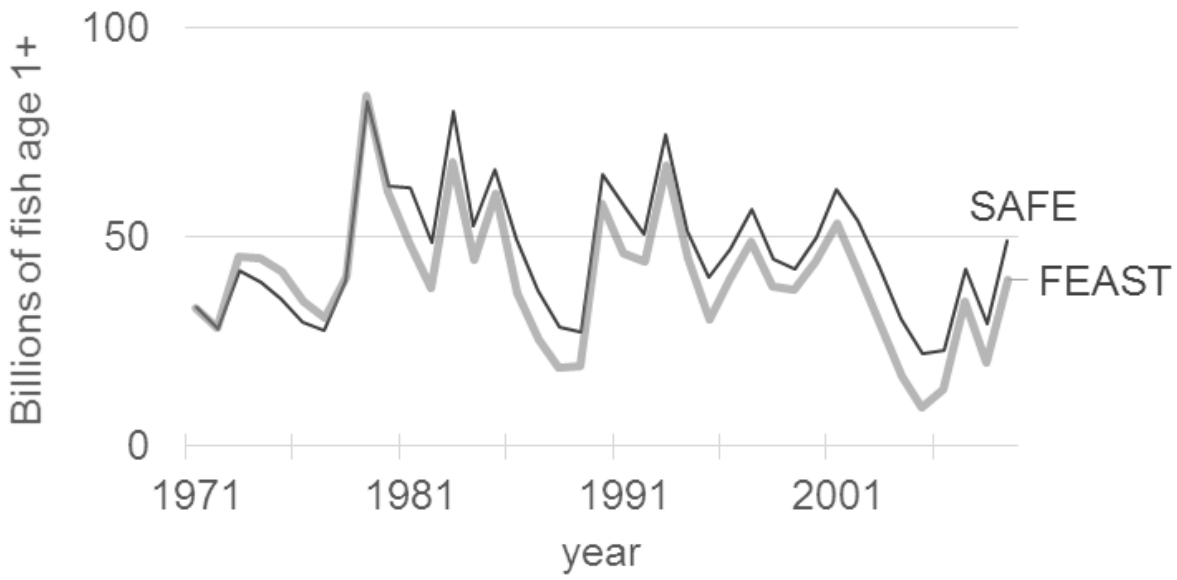
100
50
0
Billions of fish age 1+
1971
1981
1991
2001
year
SAFE
FEAST

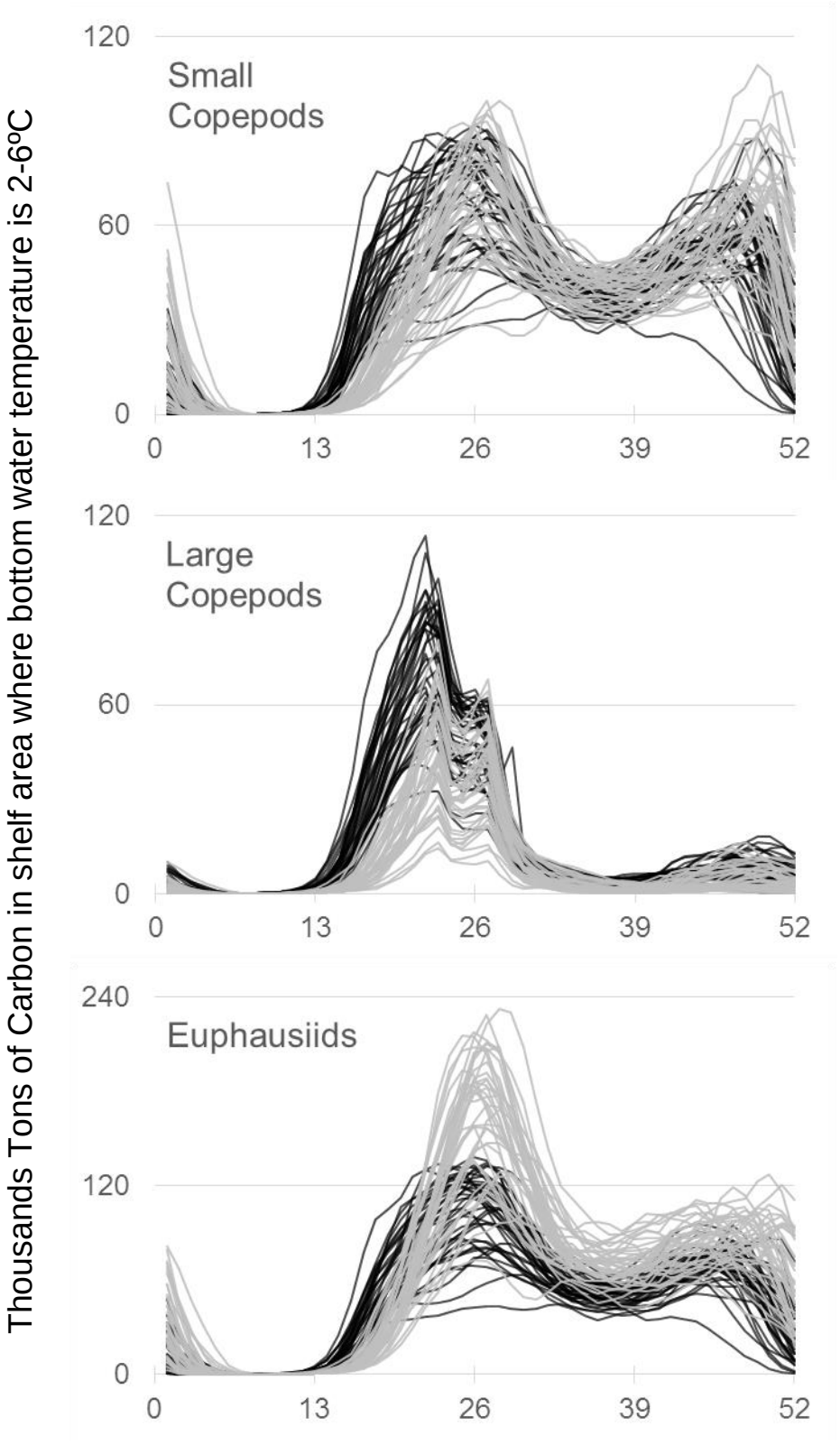
Thousands Tons of Carbon in shelf area where bottom water temperature is 2-6ºC
Small Copepods
Large Copepods
Euphausiids
120
60
0
240
120
0
0
13
26
39
52
week

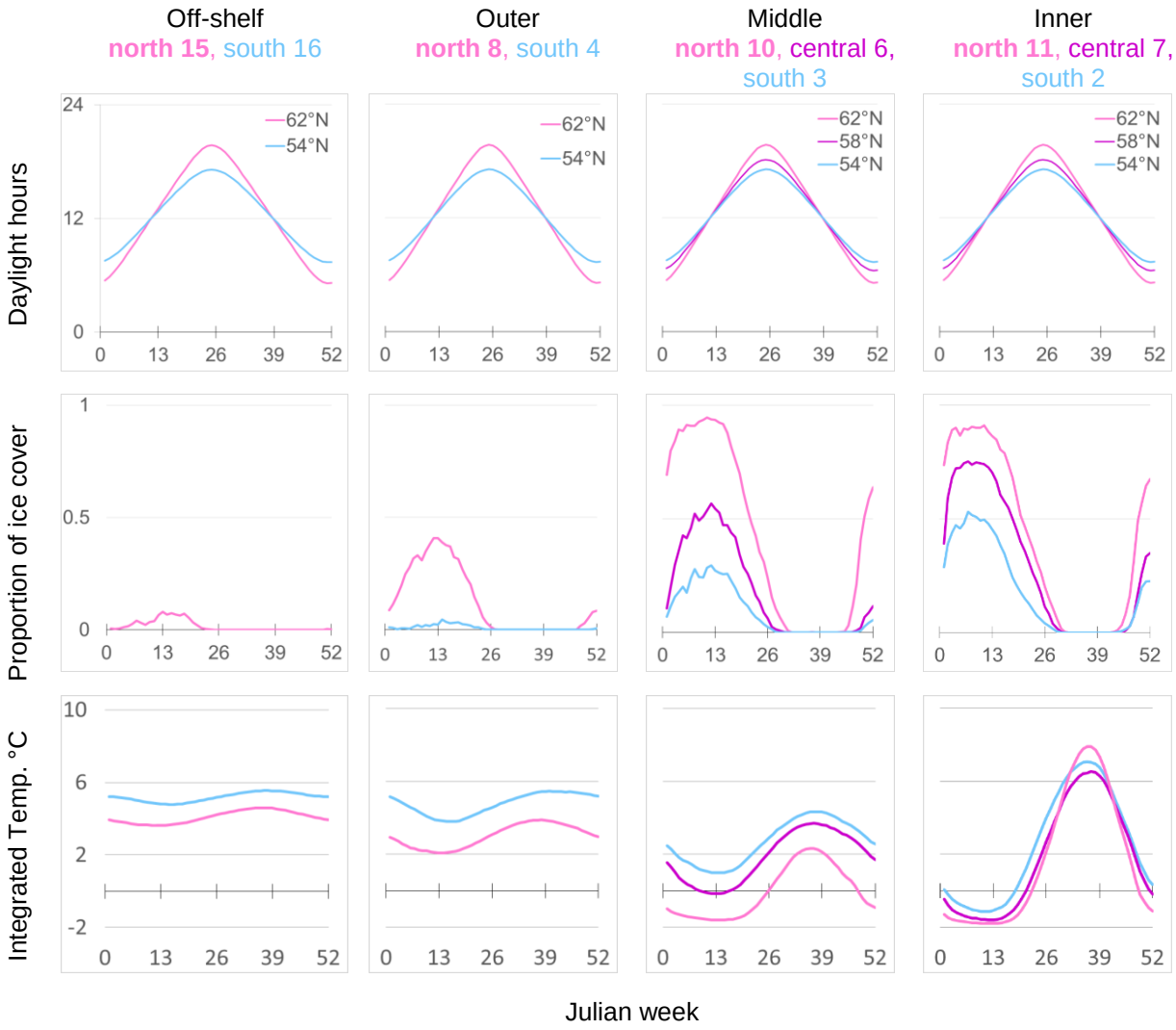
Off-shelf
north 15, south 16
Outer
north 8, south 4
Middle
north 10, central 6, south 3
Inner
north 11, central 7, south 2
Daylight hours
Proportion of ice cover
Integrated Temp. °C
62°N
58°N
54°N
24
12
0
1
0.5
10
6
2
-2
0
13
26
39
52
Julian week

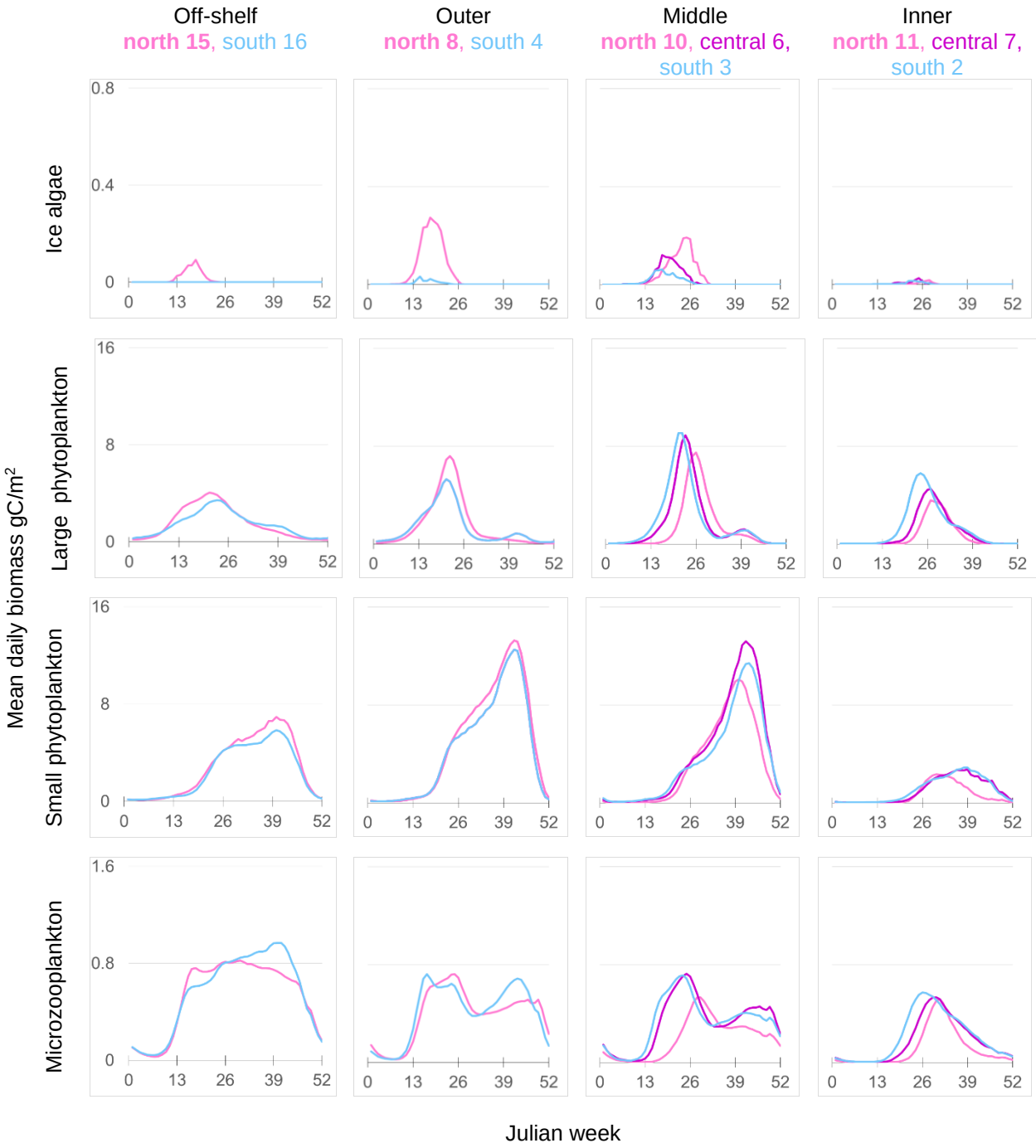
Off-shelf
north 15, south 16
Outer
north 8, south 4
Middle
north 10, central 6, south 3
Inner
north 11, central 7, south 2
Ice algae
Large phytoplankton
Small phytoplankton
Microzooplankton
Mean daily biomass gC/m²
Julian week
0
13
26
39
52
0.8
0.4
16
8
1.6

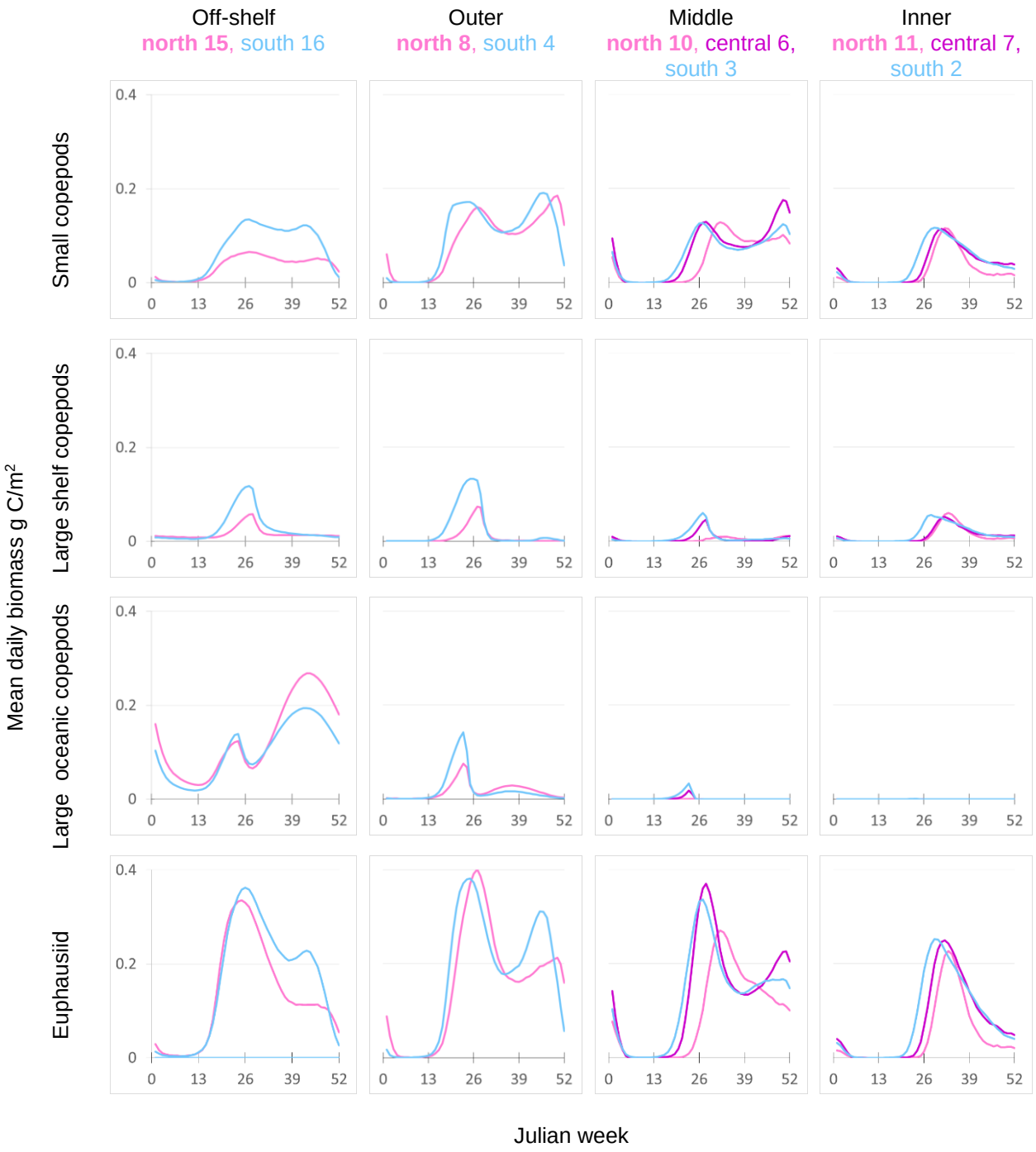
Off-shelf
north 15, south 16
Outer
north 8, south 4
Middle
north 10, central 6, south 3
Inner
north 11, central 7, south 2
Small copepods
Large shelf copepods
Large oceanic copepods
Euphausiid
Mean daily biomass g C/m²
0.4
0.2
0
0 13 26 39 52
Julian week

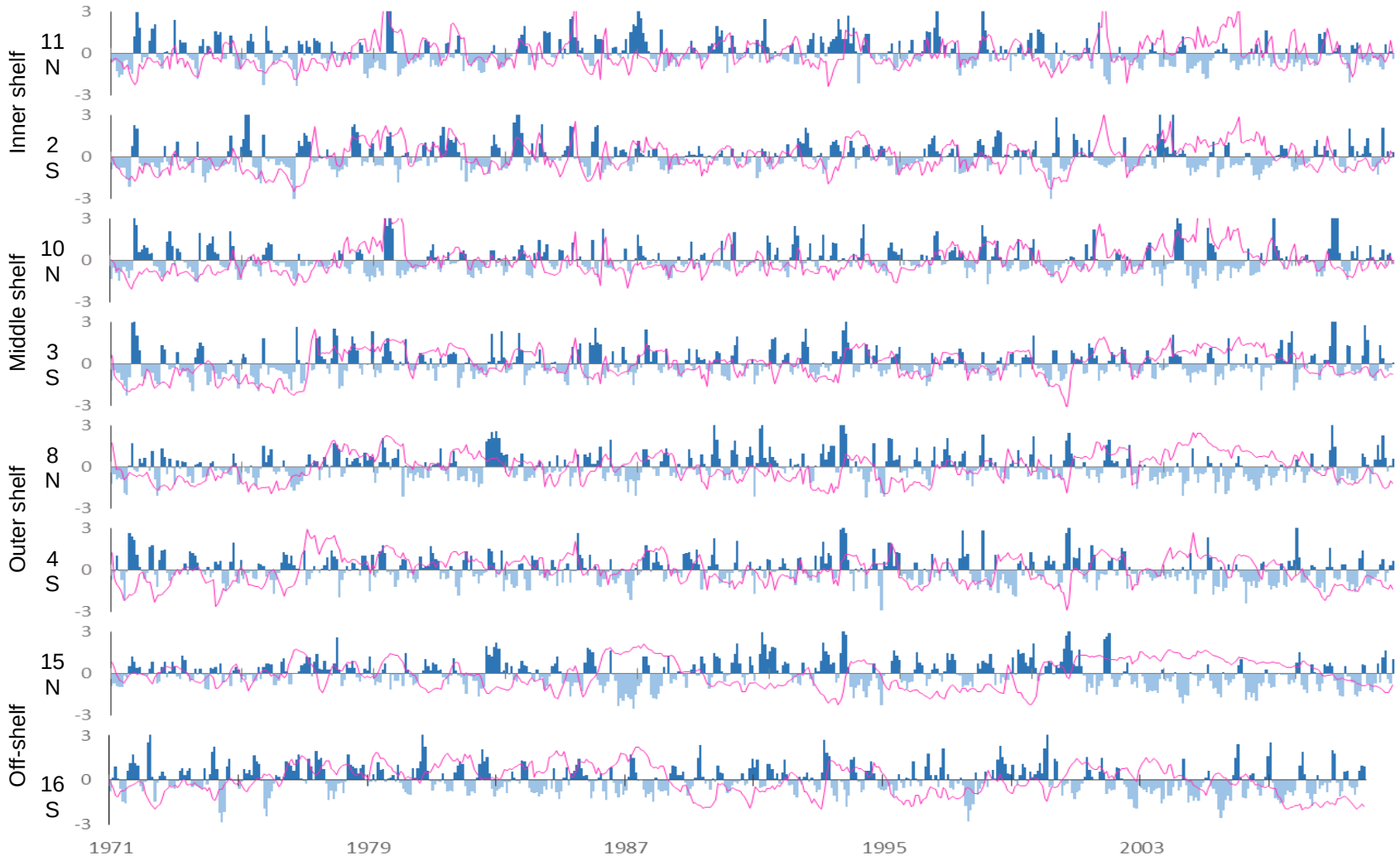
Inner shelf
11
N
2
S
Middle shelf
10
N
3
S
Outer shelf
8
N
4
S
Off-shelf
15
N
16
S
3
0
-3
1971
1979
1987
1995
2003

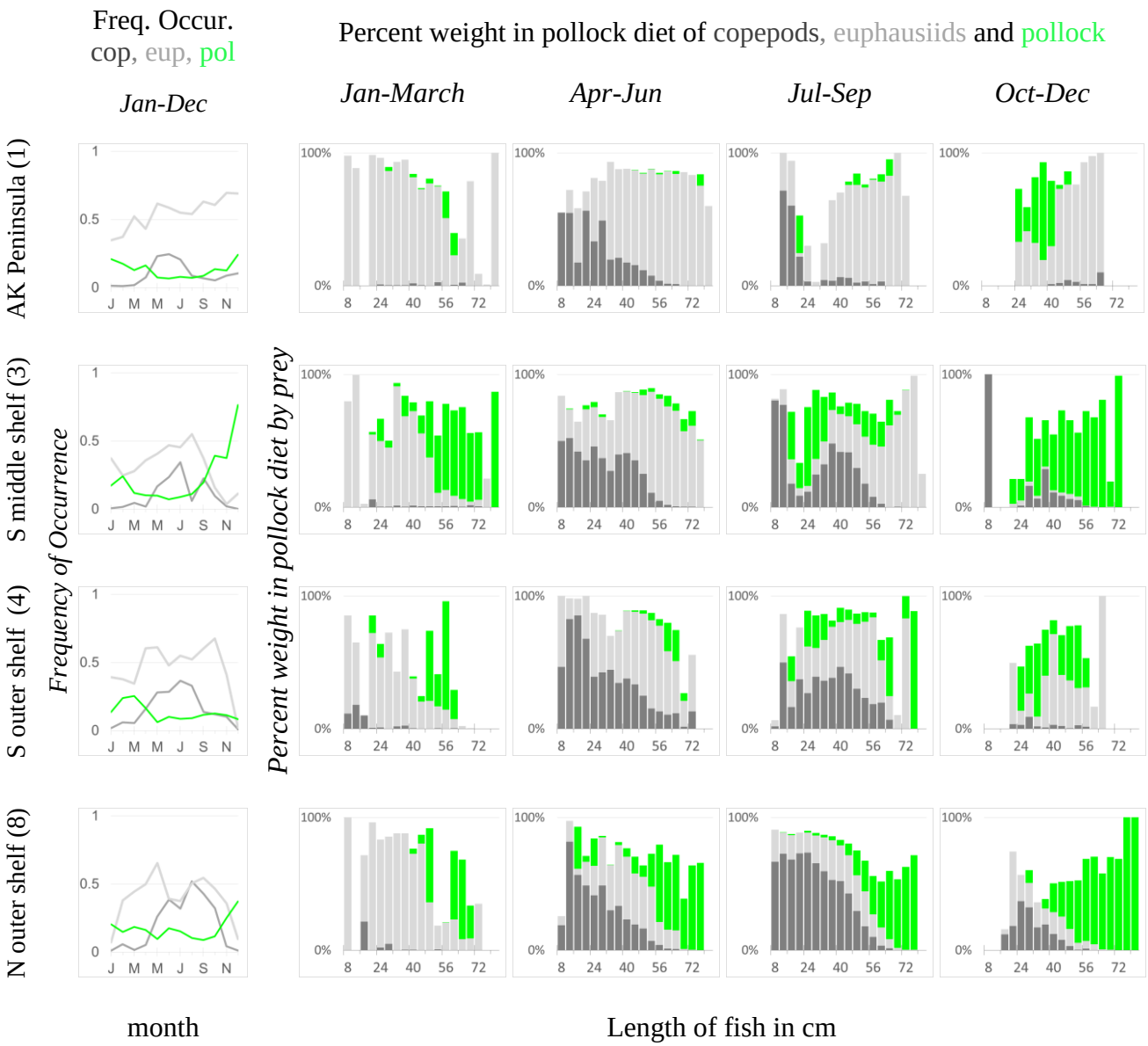
Freq. Occur.
cop, eup, pol
Percent weight in pollock diet of copepods, euphausiids and pollock
Jan-Dec
Jan-March
Apr-Jun
Jul-Sep
Oct-Dec
AK Peninsula (1)
S middle shelf (3)
S outer shelf (4)
N outer shelf (8)
Frequency of Occurrence
Percent weight in pollock diet by prey
J M M J S N
1
0.5
0
100%
0%
8 24 40 56 72
month
Length of fish in cm

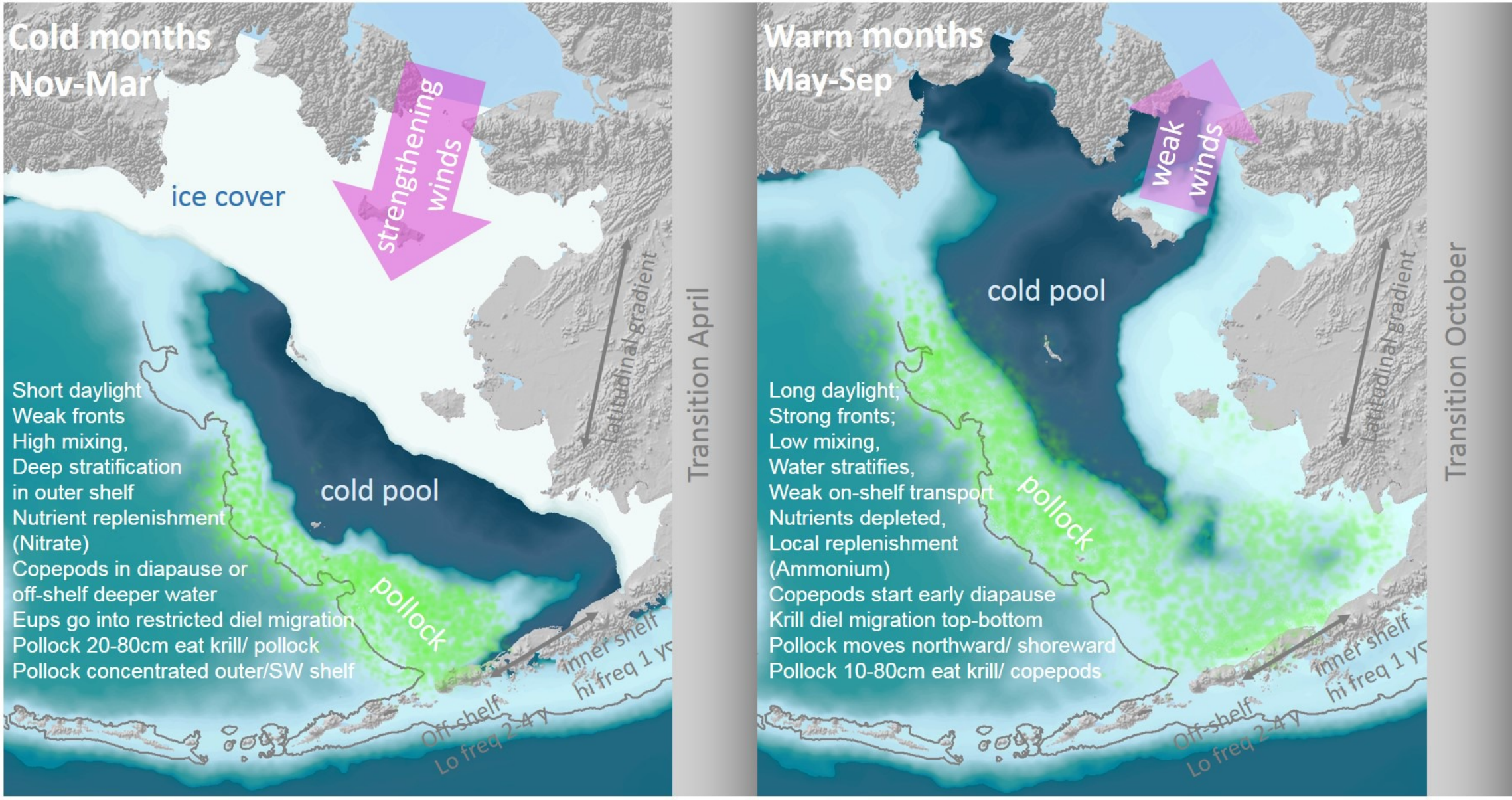
Cold months
Nov-Mar
ice cover
strengthening winds
latitudinal gradient
Short daylight
Weak fronts
High mixing,
Deep stratification
in outer shelf
Nutrient replenishment
(Nitrate)
Copepods in diapause or
off-shelf deeper water
Eups go into restricted diel migration
Pollock 20-80cm eat krill/ pollock
Pollock concentrated outer/SW shelf
cold pool
pollock
inner shelf
hi freq 1 yr
Off-shelf
Lo freq 2-4 y
Transition April
Warm months
May-Sep
weak winds
cold pool
latitudinal gradient
Long daylight;
Strong fronts;
Low mixing,
Water stratifies,
Weak on-shelf transport
Nutrients depleted,
Local replenishment
(Ammonium)
Copepods start early diapause
Krill diel migration top-bottom
Pollock moves northward/ shoreward
Pollock 10-80cm eat krill/ copepods
pollock
inner shelf
hi freq 1 yr
Off-shelf
Lo freq 2-4 y
Transition October

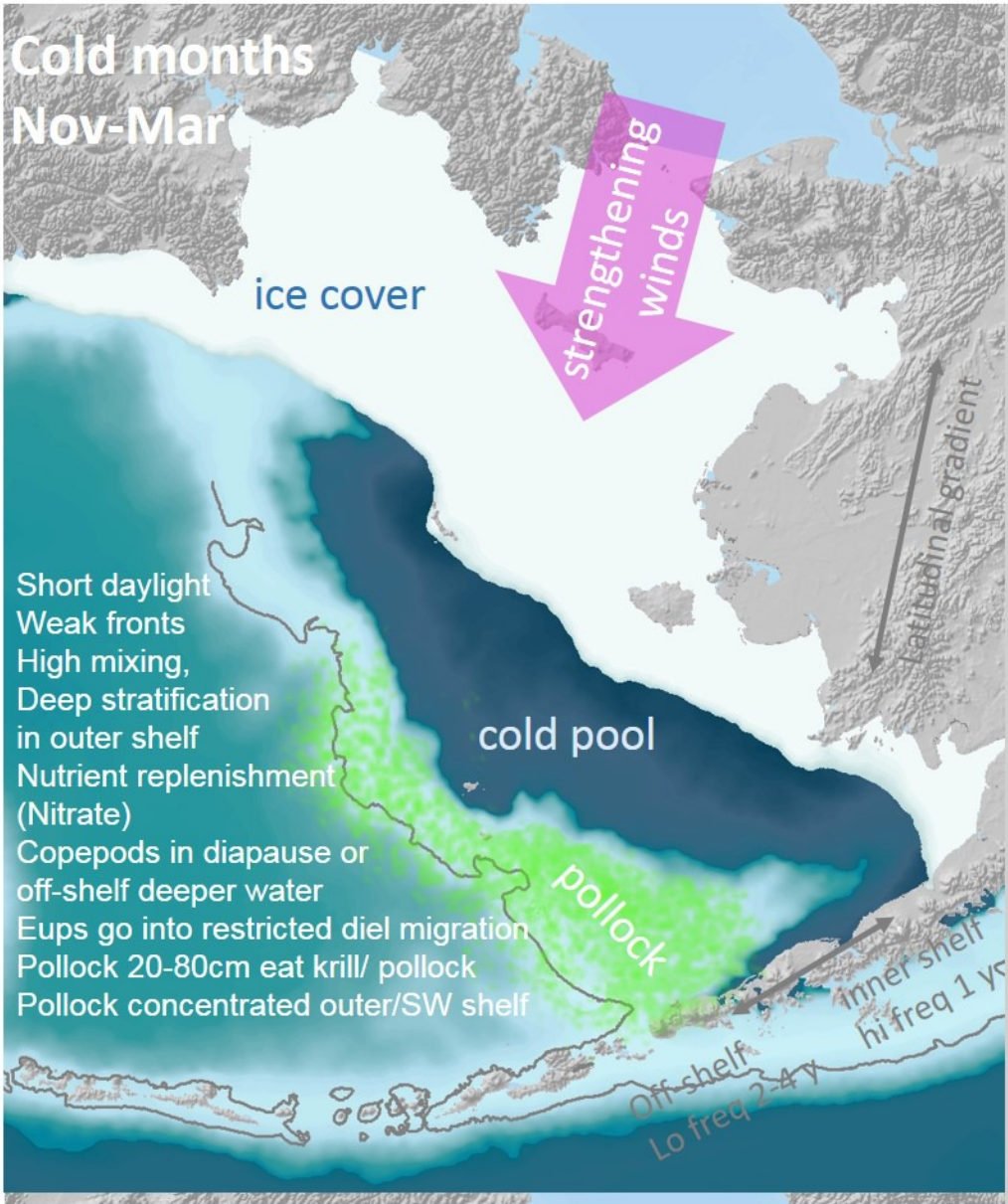
Cold months
Nov-Mar
ice cover
strengthening winds
latitudinal gradient
Short daylight
Weak fronts
High mixing,
Deep stratification
in outer shelf
Nutrient replenishment
(Nitrate)
Copepods in diapause or
off-shelf deeper water
Eups go into restricted diel migration
Pollock 20-80cm eat krill/ pollock
Pollock concentrated outer/SW shelf
cold pool
pollock
inner shelf
hi freq 1 yr
Off-shelf
Lo freq 2-4 yr
Transition April

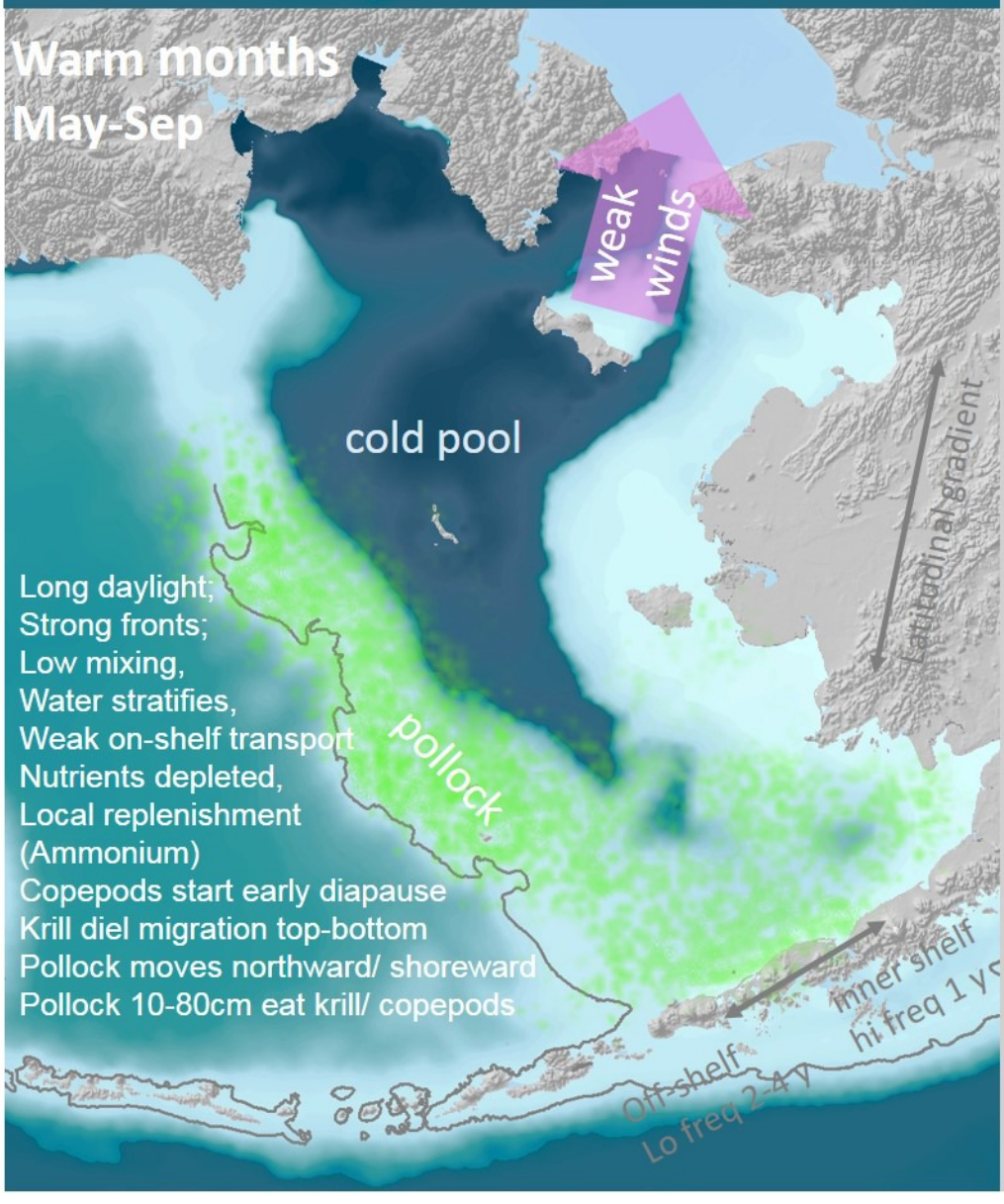
Warm months
May-Sep
weak winds
cold pool
latitudinal gradient
Long daylight;
Strong fronts;
Low mixing,
Water stratifies,
Weak on-shelf transport
Nutrients depleted,
Local replenishment
(Ammonium)
Copepods start early diapause
Krill diel migration top-bottom
Pollock moves northward/ shoreward
Pollock 10-80cm eat krill/ copepods
pollock
inner shelf
hi freq 1 yr
Off-shelf
Lo freq 2-4 yr
Transition October